10.5.1.2 Extrathoracic Deposition

The fraction of inhaled particles depositing in the ET region can be quite variable, depending on particle size, flow rate, breathing frequency and whether the breathing is through the nose or through the mouth. During exertion, the flow resistance of the nasal passages cause a shift to mouth breathing in almost all individuals, thereby bypassing much of the filtration capabilities of the head and leading to increased deposition in the lung (TB and A regions). For nose breathing, the usual technique for measuring inspiratory deposition is to draw the aerosol through the nose and out of the mouth while the subject holds his mouth open (Pattle, 1961; Lippmann, 1970; Hounam et al., 1969, 1971). The aerosol concentration is measured before it enters the nose and after it leaves the mouth. Neglecting mouth deposition during expiration, inspiratory nasal deposition can be calculated from the concentration difference. Another method to measure the nasal deposition is to use the lung as a part of the experimental system (Giacomelli-Maltoni et al., 1972; Martens and Jacobi, 1973; Rudolf, 1975). The deposition of particles in the nose is calculated from total deposition of particles in the entire respiratory tract for mouth, nose, mouth-nose and nose-mouth breathing. Because mouth deposition is not significant under the experimental conditions, this method allows the determination of nasal deposition for both inspiration and expiration.

Deposition in the mouth for expiration is normally assumed to be negligible. For inspiration, the deposition in mouth has been measured using radioactive aerosol particles (Rudolf, 1975; Lippmann, 1977; Foord et al., 1978; Stahlhofen et al., 1980; Chan and Lippmann, 1980; Stahlhofen et al., 1981, 1983). The amount of deposition is obtained from the difference of activity measurements, one immediately after exposure and the other after the deposited particles are removed with mouthwash or other means. Because the subjects in these experiments breathe through a large bore tube, the deposition via the mouth occurs predominantly in the larynx. Rudolf et al. (1984, 1986) have suggested to name this laryngeal deposition. Mouth deposition by natural mouth breathing without using a mouthpiece was measured in an earlier study by Dennis (1961) and recently by Bowes and Swift (1989) during natural oronasal breathing at moderate and heavy exercise conditions. The data showed a much greater deposition than breathing through a mouth-piece.

For $d_{ae} > 0.2$ μm, ET deposition is usually expressed as a function of $d_{ae}^2 Q$, where Q is the flow rate. This is the appropriate parameter for normalizing impaction-dominated deposition when the actual flow rates in the experimental studies are not identical. Even with this normalization, deposition data in the extrathoracic region by various workers exhibit a very large amount of scatter as shown in Figures 10-22 and 10-23, respectively, for inspiratory nasal and mouth deposition. Besides uncertainty in measurement techniques, one major source of this scatter, similar to the case of total deposition, comes from intersubject and intrasubject variabilities. The intersubject variability may arise from the difference in anatomical structure and dimensions, number of nasal hairs, breathing pattern, etc., while the intrasubject variability may be caused by the degree of mouth opening and by the nasal resistance cycle in which airflow may be redistributed from one side to the other side, by as much as 20 to 80%.

Mathematical model studies on the deposition in the nose and mouth are very limited. There have been only two attempts to determine nasal deposition during inspiration (Landahl, 1950b; Scott et al., 1978). At present, formulas useful for predicting ET deposition are derived empirically from experimental data (Pattle, 1961; Yu et al., 1981; Rudolf et al., 1983, 1984, 1986; Miller et al., 1988; Zhang and Yu, 1993). The formulas by Rudolf et al. (1983, 1984, 1986) given below, with some modification, have been adopted by the International Commission on Radiological Protection (ICRP, 1994) in their dosimetry model. Deposition efficiency via the nose (η_N) or mouth (η_M) is expressed in terms of an impaction parameter ($d_{ae}^2 Q$), as

$$\eta_N = 1 - [3.0\times10^{-4}(d_{ae}^2 Q) + 1]^{-1} , \qquad (10\text{-}22)$$

or

$$\eta_M = 1 - [1.1\times10^{-4}(d_{ae} Q^{0.6} V_T^{-0.2})^{1.4} + 1]^{-1} . \qquad (10\text{-}23)$$

where d_{ae} is in the unit of μm, Q in cm^3/s, and V_T is the tidal volume in cm^3. Equation 10-22 applies to both inspiration and expiration since the data by Heyder and Rudolf (1977) do not show a systematic difference between the two efficiencies. The

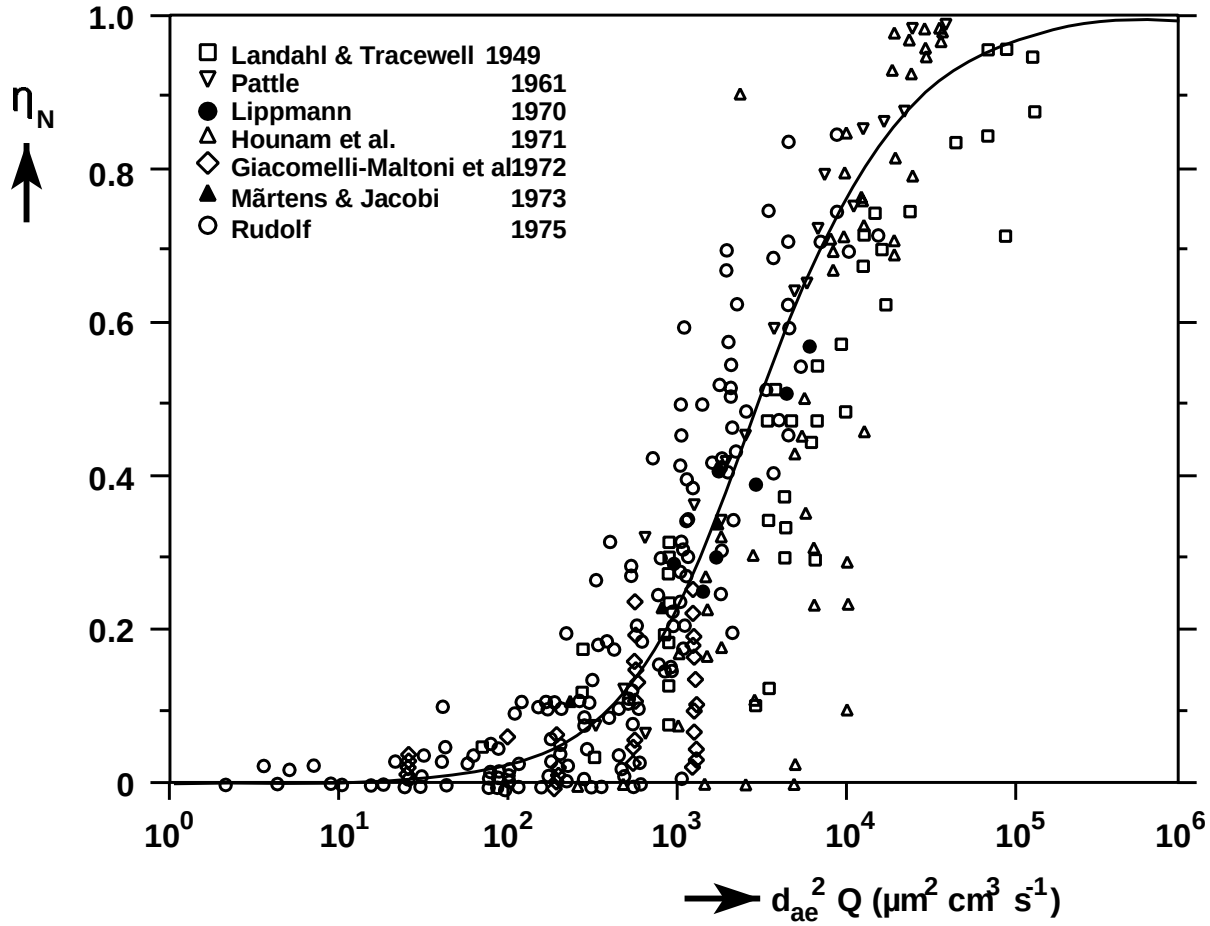

Figure 10-22. Inspiratory deposition of the human nose as a function of particle aerodynamic diameter and flow rate (d_{ae}^2Q). The curve represents Equation 10-22.

Source: Stahlhofen et al. (1988).

inclusion of V_T in Equation 10-23 is caused by the fact that the size of the ET region during mouth breathing increases with increasing flow rate and with increasing tidal volume.

For ultrafine particles (d < 0.1 μm), deposition in the ET region is controlled by the mechanism of diffusion which depends only on the particle geometric diameter, d. At this time, ET deposition for this particle size range has not been studied extensively in humans. George and Breslin (1969) measured nasal deposition of radon progeny in three subjects but the diffusion coefficient of the progeny was uncertain. Schiller et al. (1986, 1988) later obtained inspiratory nasal deposition from total deposition measurements using a nose in -

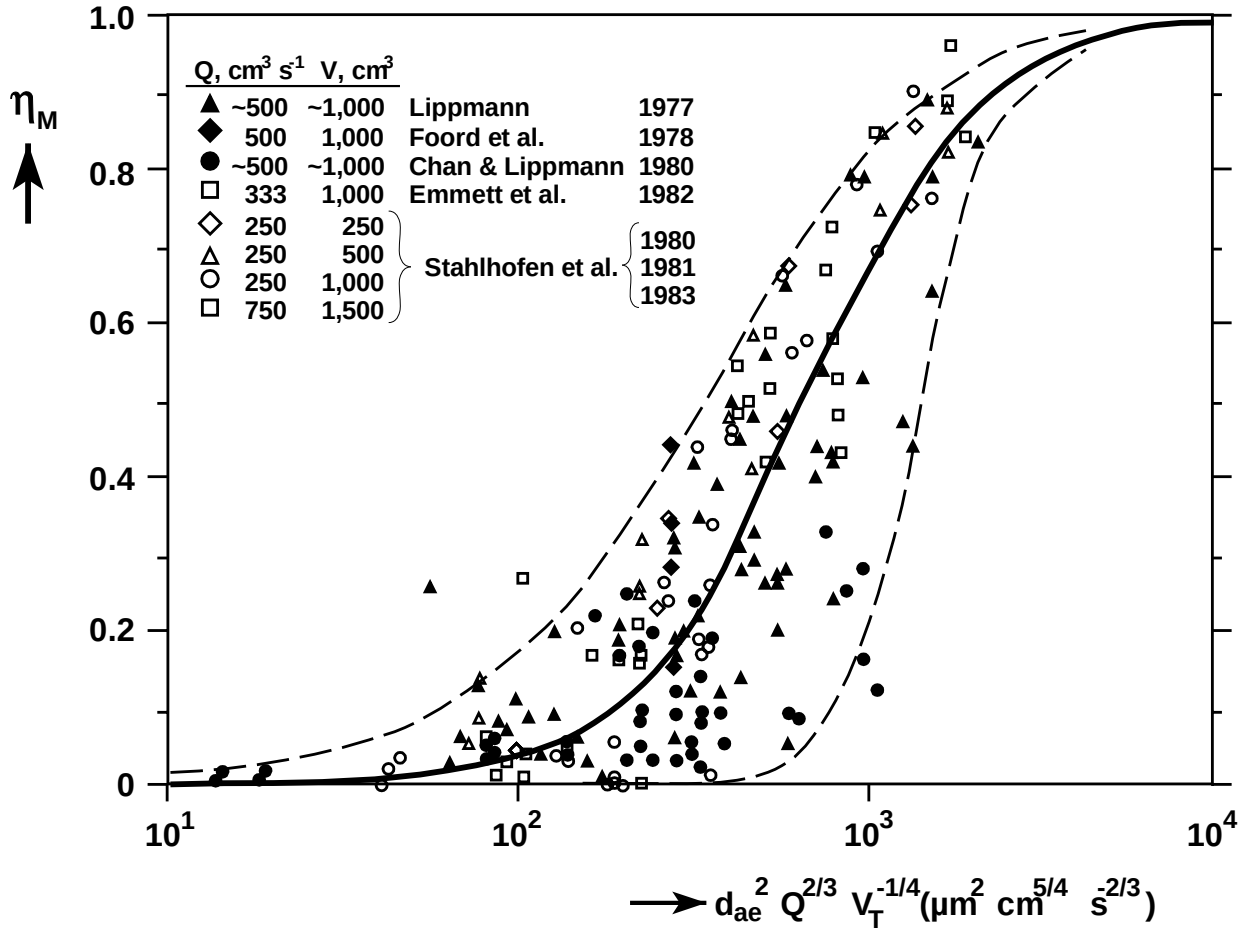

Figure 10-23. Inspiratory extrathoracic deposition data in humans during mouth breathing as a function of particle aerodynamic diameter, flow rate, and tidal volume ($d_{ae}^2 Q^{2/3} V_T^{-1/4}$). The curve represents Equation 10-23.

Source: Stahlhofen et al. (1988).

mouth out and mouth in-nose out maneuver. However, their data cannot be considered reliable because mouth deposition is not negligible compared to nose deposition.

The only data available to date for ET deposition of ultrafine particles are from cast measurements (Cheng et al., 1988, 1990, 1993; Yamada et al., 1988; Gradon and Yu, 1989; Swift et al., 1992). Figure 10-24 shows these data on inspiratory nasal deposition from several laboratories reported by Swift et al. (1992) as a function of the diffusion parameter, $D^{1/2}Q^{-1/8}$, where *D* is the particle diffusion coefficient in cm^2/sec and Q is the flow rate in L/min. Swift et al. (1992) also proposed an equation to fit the data in the form

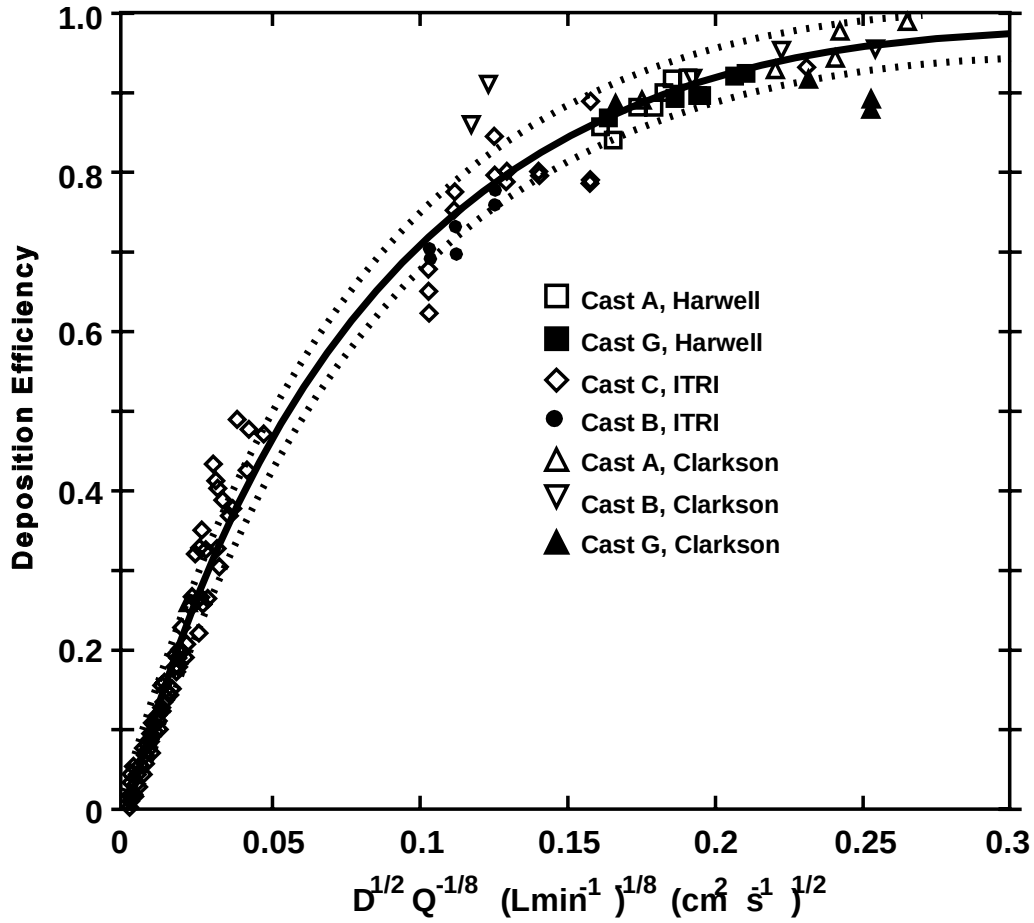

Figure 10-24. Inspiratory deposition efficiency data and fitted curve for human nasal casts plotted versus $Q^{-1/8}D^{1/2}$ $(Lmin^{-1})^{-1/8}(cm^2s^{-1})^{1/2}$. The solid curve represents Equation 10-24 and the dotted lines are 95% confidence limits on the mean.

Source: Swift et al. (1992).

$$\eta_N = 1 - \exp[-12.65 D^{1/2} Q^{-1/8}], \qquad (10\text{-}24)$$

which was adopted by ICRP66 in the 1994 model. Expiratory nasal deposition for particles between 0.005 μm to 0.2 μm was found to have the same trend as Figure 10-24 but was approximately 10% higher than the inspiratory nasal deposition (Yamada et al., 1988). Cheng et al. (1993) derived the following empirical equations to fit the data for expiratory nasal deposition

$$\eta_N = 1 - \exp[-15.0 D^{1/2} Q^{-1/8}]. \quad (10\text{-}25)$$

Diffusional deposition in human oral casts was found to be smaller than that in nasal casts (Cheng et al., 1990). Based upon these data, Cheng et al. (1993) derived the following equation for oral deposition

$$\eta_M = 1 - \exp(-10.3 D^{1/2} Q^{-1/8}), \quad (10\text{-}26)$$

on inspiration, and

$$\eta_M = 1 - \exp(-8.51 D^{1/2} Q^{-1/8}), \quad (10\text{-}27)$$

for deposition on expiration. Contrary to nasal deposition, deposition in the mouth is slightly higher for inspiration than for expiration. Figure 10-25 shows the inspiratory oral deposition data and Equation 10-26.

ICRP66 (1994) took a more conservative view of the experimental data on deposition of small particles in the oral passageway. Oropharyngeal deposition for mouth breathing was assumed to be only half the value for nose breathing so that

$$\eta_m = 1 - \exp(-6.33 D^{1/2} Q^{-1/8}). \quad (10\text{-}28)$$

10.5.1.3 Tracheobronchial Deposition

Particles escaping from deposition in the ET region enter the lung, but their regional deposition in the lung cannot be precisely measured. All the available regional deposition data have been obtained from experiments with radioactive labeled poorly soluble particles above 0.1 μm in diameter. The amount of activity retained in the lung as a function of time normally exhibits a fast and slow decay component that have been identified as mucociliary and macrophage clearance. Since the tracheobronchial airways are ciliated, the rapidly

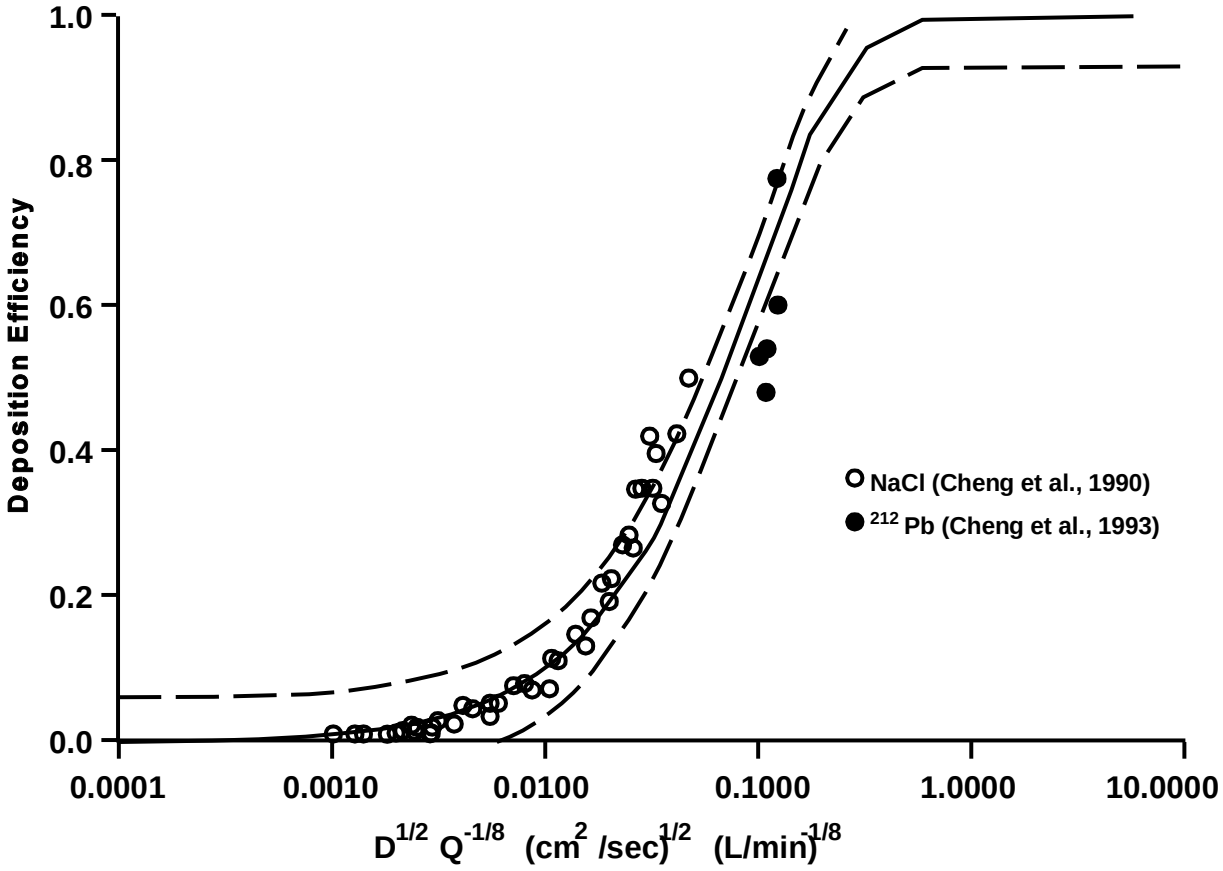

Figure 10-25. Inspiratory deposition efficiency data in human oral casts plotted versus flow rate and particle diffusion coefficient [$Q^{-1/8}D^{1/2}$ $(Lmin^{-1})^{-1/8}$ $(cm^2s^{-1})^{1/2}$]. The solid curve represents Equation 10-26 and the dotted lines are the 95% confidence limits.

Source: Cheng et al. (1993).

cleared fraction of initial activity can be considered as a measure of the amount of material deposited in the TB region, whereas the slowly cleared fraction corresponds to the material deposited in the A region. However, there is experimental evidence that a significant fraction of material deposited in the TB region is retained much longer than 24 h (Stahlhofen et al., 1986a,b; Scheuch and Stahlhofen, 1988; Smaldone et al., 1988). This may be caused by the fact that the TB airway surface is lined with ciliated epithelium, but not all of the ciliated epithelium is covered with mucus all the time (Stahlhofen et al., 1989). Other mechanisms for prolonged TB clearance include phagocytosis by airway macrophages and

deposition of particles further down into the A region due to mixing of flow during inspiration. Thus, TB and A deposition measured based upon the clearance of radioactive labeled particles have been suggested as the "fast-cleared" and "slow-cleared" thoracic deposition (Stahlhofen et al., 1989).

Figure 10-26 shows the data from various investigators (Lippmann, 1977; Foord et al., 1978; Chan and Lippmann, 1980; Emmett et al., 1982; and Stahlhofen et al., 1980, 1981, 1983) on TB deposition or fast-cleared thoracic deposition for mouth breathing as a function of d_{ae} reported by Stahlhofen et al. (1989). Again, the data are quite scattered due to differences in experimental technique and intersubject and intrasubject variabilities that have been cited previously. Another cause for the scatter is from the difference in the flow rate employed by various studies. For $d_{ae} > 0.5$ μm, deposition in the TB region is caused by both impaction and sedimentation. Whereas the impaction deposition is governed by the parameter d_{ae}^2Q, sedimentation deposition is controlled by the parameter d_{ae}^2/Q. It is therefore not possible to have a single relationship between deposition and d_{ae} for different flow rates.

Data in Figure 10-26 show that TB deposition does not increase monotonically with d_{ae}. A higher d_{ae} leads to a greater ET deposition and consequently a lower TB deposition. For the range of flow rates employed in various studies, the maximum TB deposition occurs at about 4 μm d_{ae}. It is also seen that the data by Stahlhofen et al. (1980, 1981, 1983) in Figure 10-26 are considerably lower than those from other investigators. Chan and Lippmann (1980) cited two possible reasons for this difference. One was that Stahlhofen and coworkers used constant respiratory flow rates in their studies as opposed to the variable flow rates used by others. The second reason was that different methods of separating the initial thoracic burden into TB and A regions were used. Stahlhofen et al. (1980) extrapolated the thoracic retention values during the week after the end of fast clearance back to the time of inhalation; they considered A deposition to be the intercept at that time, with the remainder of the thoracic burden considered as TB deposition. This approach yields results similar to, but not identical with, those obtained by treating TB deposition as equivalent to the particles cleared within 24 h.

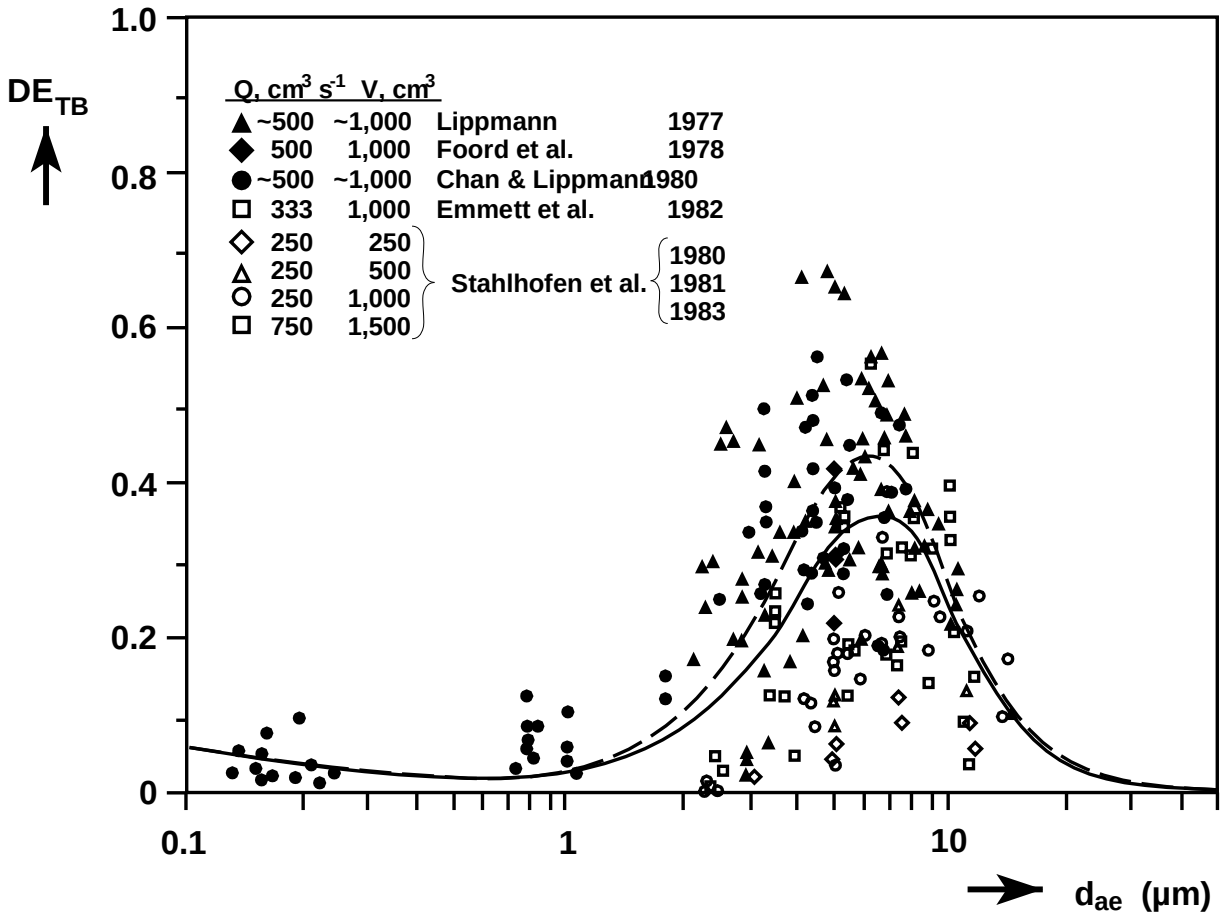

Figure 10-26. Tracheobronchial deposition data in humans at mouth breathing as a function of particle aerodynamic diameter (d_{ae}). The solid curve represents the approximate mean of all the experimental data; the broken curve represents the mean excluding the data of Stahlhofen et al.

Source: Stahlhofen et al. (1988).

10.5.1.4 Alveolar Deposition

The A deposition data as a function of d_{ae} for mouth breathing are shown in Figure 10-27. These data are from the same studies that reported TB deposition in Figure 10-25 but there is a better agreement between different studies than with the TB data. Alveolar deposition is favored by slow and deep breathing. The data of Stahlhofen et al. (1980, 1981, 1983) at 1000 cm^3 tidal volume and 250 cm^3/sec flow rate thus are higher than other data. Figure 10-27 also shows (1) that A deposition reaches the maximum at about

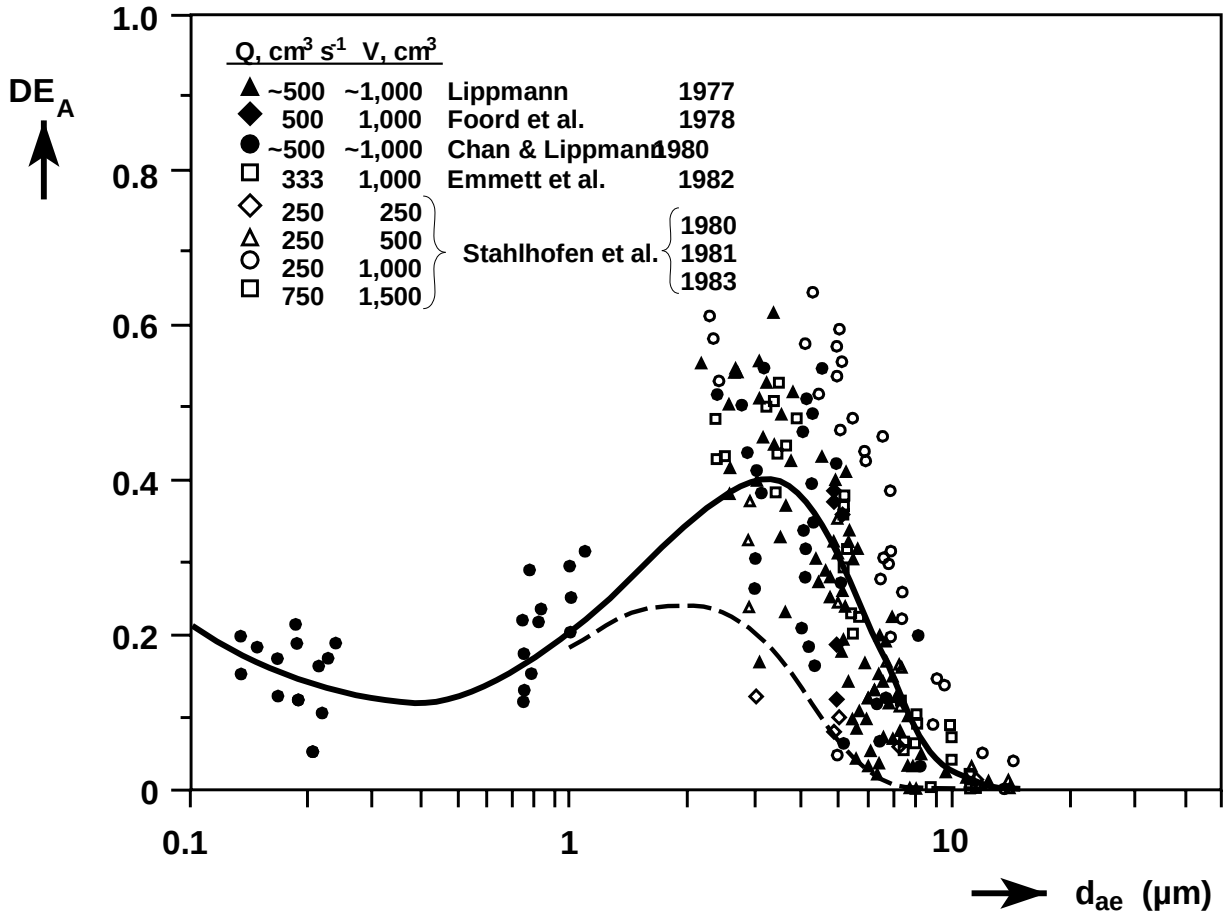

Figure 10-27. Alveolar deposition data in humans as a function of particle aerodynamic diameter (d_{ae}). The solid curve represents the mean of all the data; the broken curve is an estimate of deposition for nose breathing by Lippmann (1977).

Source: Stahlhofen et al. (1988).

3.5 µm d_{ae} and (2) that for d_{ae} between 0.2 µm and 1.0 µm, A deposition does not show significant change although a minimum deposition may occur near 0.5 µm.

By switching from mouth breathing to nose breathing, alveolar deposition will decrease. Lippmann (1977) made an estimate by analysis of the difference in the ET deposition for nose and mouth breathing. The nose breathing (dashed line) result is also shown in Figure 10-26. For d_{ae} greater than 7 µm, practically no particles deposit in the A region in this breathing mode.

During exercise, most subjects switch from nose breathing to breathing partly through the mouth (Niinimaa et al., 1981). The amount of inhaled material that deposits in the lungs is affected because the mouth and nose have different filtration efficiencies. Niinimaa et al. (1981) found that in thirty subjects, twenty switched to oro-nasal breathing (normal augmenters), typically at a ventilation rate of about 35 L/min, five continued to breathe through the nose, and the rest who were habitual mouth breathers breathed oro-nasally at all levels of exercise. These data were reviewed by Miller et al. (1988) and used to estimate thoracic deposition (TB and A deposition) at different ventilation rates. At higher ventilation rates, Miller et al. (1988) predicted little difference in thoracic deposition between normal augmenters and mouth breathers, but for ventilation rates less than 35 L/min they predicted substantially lower deposition in normal argumenters compared to mouth breathers. Based upon this finding, ICRP (1994) recommended a different breathing pattern for normal augmenters and mouth breathers that typifies the breathing habits of adult males as a function of ventilation rate. The split in airflow for the recommended breathing patterns by ICRP (1994) is shown in Figure 10-28. Table 10-10 provides the same information on the percentages of total ventilatory airflow passing through the nose versus mouth at reference levels of physical exertion for a normal augmenter and a mouth breather adult male. These are the same levels of exercise and values for fraction of nasal ventilatory airflow used to construct the activity patterns in Section 10.7. In the absence of specific data, it must be assumed that a similar breathing pattern applies to young healthy subjects at equivalent levels of exercise. Alveolar deposition at different ventilation rates can be estimated from Figure 10-28 or Table 10-10. For example, a mouth breather doing light exercise ($\dot{\mathbf{V}}_E$ = 1.5 m^3/h) has about 40% ventilatory air-flow passing through the nasal route. At a particle size of 2 μm $d_{ae,}$ Figure 10-28 gives, respectively, 0.24 and 0.36 A deposition for mouth and nose breathing. Thus, the resultant A deposition at this ventilation rate is $0.4 \times 0.36 + 0.6 \times 0.24 = 0.288$.

10.5.1.5 Nonuniform Distribution of Deposition and Local Deposition Hot Spots

The deposition data in different regions of the respiratory tract do not provide information on deposition nonuniformity in each region and local deposition intensity at a specific site. Such information may be of great importance from a toxicology perspective.

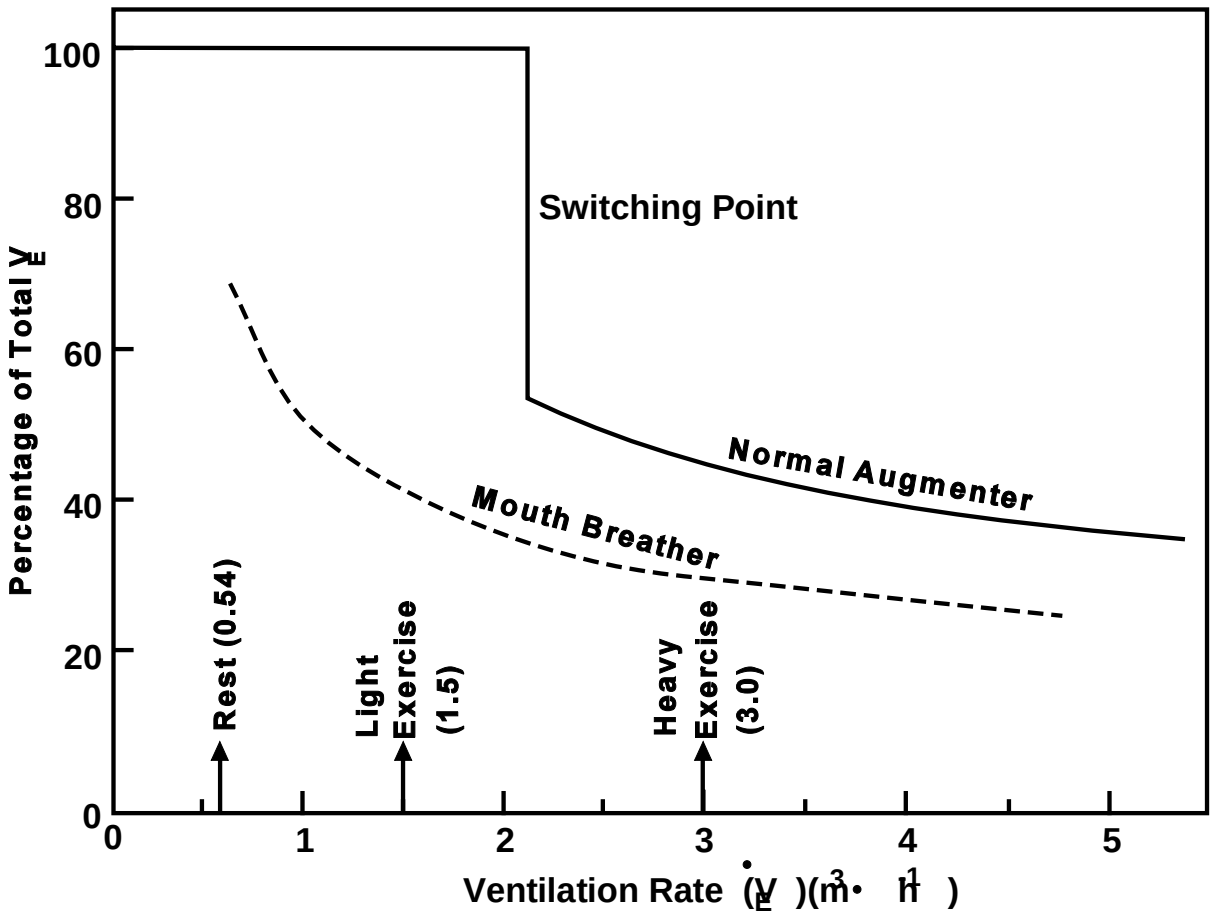

Figure 10-28. Percentage of total ventilatory airflow passing through the nasal route in human "normal augmenter" (solid curve) and in habitual "mouth breather" (broken curve).

Source: International Commission on Radiological Protection (ICRP66, 1994).

TABLE 10-10. FRACTION OF VENTILATORY AIRFLOW PASSING THROUGH THE NOSE IN HUMAN "NORMAL AUGMENTER" AND "MOUTH BREATHER"[a]

	F_n	
Level of Excertion	Nasal Augmenter	Mouth Breather
Sleep	1.0	0.7
Rest	1.0	0.7
Light exercise	1.0	0.4
Heavy exercise	0.5	0.3

[a](ICRP66, 1994) as derived from Miller et al. (1988).

Because airway structure and its associated air flow patterns are exceedingly complex (Chang and Menon, 1993), and ventilation distribution of air in different parts of the lung is uneven (Milic-Emili et al., 1966), it is expected that particle deposition patterns in ET, TB, and A regions are highly nonuniform. Fry and Black (1973) measured regional deposition in the human nose using radiolabelled particles and found that most of deposition occurred in the anterior region of the nose. Schlesinger and Lippmann (1978) found nonuniform deposition in the trachea to be caused by the airflow disturbance of the larynx. In a single airway bifurcation model, measurements show that deposition occurs principally around the carinal ridge (e.g., Bell and Friedlander, 1973; Lee and Wang, 1977); Martonen and Lowe, 1983; Kim and Iglesias, 1989 a,b). A similar result was observed in the alveolar duct bifurcations in rats and mice (Brody and Roe, 1983). Figure 10-29 shows the data on local deposition pattern obtained by Kim and Iglesias (1989) and Kim et al. (1989) in a bifurcating tube for both inspiration and expiration. The peak deposition occurs in the daughter tube during inspiration and the parent tube during expiration, but always near the carinal ridge. In addition, airways are not smooth tubes. More recently, Martonen et al. (1994 a,b,c) have called attention to the existence of cartilaginous rings on the wall of airways in the tracheobronchial region. Using a numerical analysis, they showed that such surface structure can lead to a considerable alteration of the flow pattern and enhancement of deposition.

Deposition measurements in small laboratory rodents (Raabe et al., 1977) also showed differences in lobar distribution with up to 60 percent higher deposition than the average in the right apical lobe (corresponding to the human upper lobe). The difference was greater for large particles than for small particles. Raabe et al. (1977) further showed that these differences in relative lobar deposition were related to geometric mean number of airway bifurcations between trachea and terminal bronchioles in each lobe for rats and hamsters. Since similar morphologic differences occur in the human lungs, nonuniform lobar distribution should also occur.

10.5.1.6 Approaches to Deposition Modeling

Mathematical models of lung deposition have been developed in recent years to help interpret experimental data and to make predictions of deposition for cases where data are not available. A review of various mathematical models was given by Morrow and Yu

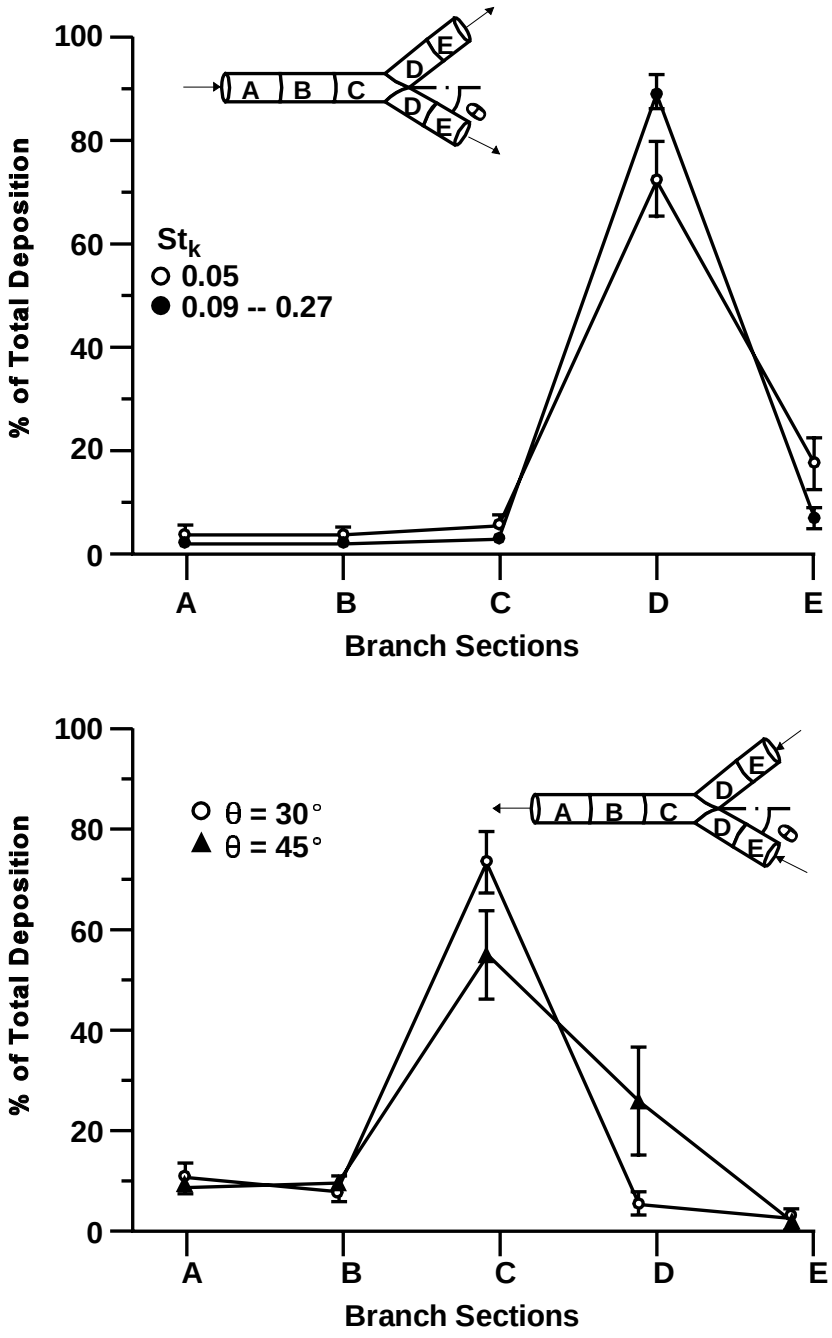

Figure 10-29. Local deposition pattern in a bifurcating tube for inhalation (top panel) and exhalation (bottom panel). Deposition in each section is expressed as a percent of total deposition for the entire model. Symbols and error bars in the top panel represent means and standard deviations of the θ = 30° and 45°. Symbols and error bars in the bottom panel represent means and standard deviations of the entire data obtained in the Stokes number range from 0.05 to 0.28.

Source: Kim and Iglesias (1989); Kim et al. (1989).

(1993). There are three major elements involved in mathematical modeling. First, a model of airways simulating the real structure must be specified. Secondly, deposition efficiency in each airway due to various mechanisms must be derived. Finally, a computational procedure must be developed to account for the transport and deposition of the particles in the airways.

Three different approaches have been used in the mathematical modeling. The first approach is a compartmental model first formulated by Findeisen (1935). Starting with the trachea, Findeisen divided the airways into nine compartments based upon the anatomical structure. Particles which did not deposit in one compartment remained airborne and transported to the next compartment for deposition. Findeisen's lung model and analysis were later modified by Landahl (1950a, 1963) and Beeckmans (1965). Detailed calculations of regional deposition with additional consideration of nasal deposition based upon the Findeisen-Landahl-Beeckmans theory were later published in a report by the Task Group on Lung Dynamics (TGLD) in 1966.

Because of advancement in measuring techniques, refined airway models have become available (as discussed in Section 10.2). Several new models based upon the compartmental analysis have been proposed (e.g., Gerrity et al., 1979; Yeh and Schum, 1980; Martonen and Graham, 1987). The expressions used for deposition efficiency of each compartment differed somewhat in these models. In the absence of any careful comparison with the experimental data, it is difficult to assess the applicability of these models to deposition prediction. However, one difficulty often encountered in the compartmental model is the derivation of deposition efficiency in each airway for combined mechanisms of impaction, sedimentation and diffusion. A commonly used assumption is that each deposition mechanism is independent, thus the joint efficiency can be written in the form

$$\eta = 1 - (1 - \eta_I)(1 - \eta_S)(1 - \eta_D), \qquad (10\text{-}29)$$

where η_I, η_S, and η_D are, respectively, deposition efficiency in an airway or compartment by the individual mechanisms of impaction, sedimentation and diffusion, and η is the joint efficiency. Yu et al. (1977) have shown, in a detailed mathematical analysis of a combined sedimentation and diffusion problem, that the above equation is an inaccurate expression for deposition when η_S and η_D are not small and have about the same magnitude. Another

difficulty in the compartmental model is that the air-mixing effect (i.e., mixing of tidal air and lung air) on deposition cannot be easily accounted for. Such an effect is important for transient exposure. However, the compartmental model is easy to formulate and to understand conceptually.

The second approach to deposition modeling was put forward by Yu and coworkers (Taulbee and Yu, 1975; Yu, 1978; Yu and Diu, 1983) and later by Egan and Nixon (1985, 1989). In this approach, the many generations of airways are viewed as a chamber shaped like a trumpet. The cross-sectional area of the chamber varies with airway depth measured from the beginning of the trachea, according to anatomical data. The concentration of inhaled particles in the chamber as a function of airway depth and time during breathing is described by a convective diffusion equation with a loss-term accounting for airway deposition. This equation can be solved either exactly (without longitudinal diffusion) or numerically with appropriate initial and boundary conditions. Deposition at different sites in the airways is then calculated once the concentration is known.

The deposition model formulated in this manner has some advantages over the compartmental model. The use of differential airway length in the model allows the joint deposition efficiency per unit airway length to be the superposition of efficiencies by each individual mechanism. Variation of airway dimensions during breathing is accounted for in the model. The model is time-dependent and can thus be applied to any breathing pattern and transient exposure condition. Air-mixing and uneven airway path lengths can be accounted for with the use of an equivalent longitudinal diffusion term in the convective-diffusion equation. Finally, in the case of no longitudinal diffusion, the exact solution of the convective-diffusion is obtainable, thus reducing the time required for calculating deposition.

The airway geometry of the human lung is not identical within a population. In a given lung, the dimension of the airways in a specified generation is also not uniform and the bifurcation is not symmetric (Weibel, 1963). The above two modeling approaches have been extended to account for the randomness of airway geometry (Yu et al., 1979; Yu and Diu, 1982a,b; Koblinger and Hofmann, 1990; Hofmann and Koblinger, 1990). Yu and Diu (1982b) compared their modeling results with total and regional deposition data of Stahlhofen et al. (1981) and Heyder et al. (1982) for controlled breathing and suggested that differences

in lung morphology were probably the principal cause for intersubject variability in deposition.

Another approach to deposition modeling is an empirical one proposed by Rudolf et al. (1983, 1984, 1986, 1990) similar to that developed for ET deposition. This model considers the lung as a series of two filters representing the TB and A regions of the lung. The model requires no assumptions about airway geometry, airflow pattern and distribution, or particle deposition efficiency in each airway. However, the construction of the model relies heavily on experimental data of regional deposition for a wide range of particle sizes (monodisperse) and breathing conditions. These data are not always available. An additional difficulty in empirical modeling is the development of deposition equations in each region for combined deposition mechanisms. As discussed earlier, impaction, sedimentation and diffusion deposition depend, respectively, on the parameters d_{ae}^2Q, D_{ae}^2/Q and D/Q, where D is a function of particle geometric diameter. It is a very difficult task to come up with an equation for deposition in terms of these parameters which can match all experimental data. Furthermore, because only a few compartments are used in the empirical model, more detailed deposition information such as deposition at a specific airway generation cannot be predicted. However, as mentioned, with an empirical model the geometry and relative importance of mechanisms and airflow splits are all "correct" in the subjects tested and are reflected in the measured deposition. This may be an advantage over theoretical models that must rely on extremely limited information on geometry. As described in Appendix 10A, the ICRP based their 1994 model of respiratory tract deposition on a theoretical calculation of the type introduced by Taulbee and Yu (1975), which was found to be consistent with the experimental data taken as a whole. However, for mathematical simplicity in applying the results of these complex calculations, which included the effects of airway dimension scaling for subject gender and age, the ICRP developed a set of algebraic expressions to represent regional lung deposition in terms of the controlling parameters, i.e., particle diameter, density, shape factor, breathing mode (nose or mouth), tidal volume, respiratory frequency, functional residual capacity, gender, and subject height.

10.5.2 Laboratory Animals

Since much information concerning inhalation toxicology is collected from laboratory animals, the comparative regional deposition in these laboratory animals must be considered to help interpret, from a dosimetric viewpoint, the possible implications of animal toxicological results for humans. In evaluating deposition studies in terms of interspecies extrapolation, it is not adequate to express the amount of deposition merely as a percentage of the total inhaled. For some particle sizes, regional deposition in humans and laboratory animals may be quite similar and appears to be species independent (McMahon et al., 1977; Brain and Mensah, 1983). However, different species exposed to identical particles at the same exposure concentration will not receive the same particle mass per unit exposure time because of their differences in tidal volume and breathing rate. In addition, because of differences in the lung weight and airway surface area, the amount of deposition normalized to these quantities is also very different between species.

It is difficult to systematically compare interspecies deposition patterns obtained from various reported studies, because of variations in experimental protocols, measurement techniques, definitions of specific respiratory tract regions, and so on. For example, tests with humans are generally conducted under protocols that standardize the breathing pattern, whereas those using laboratory animals involve a wider variation in respiratory exposure conditions (for example, spontaneous breathing versus ventilated breathing as well as various degrees of sedation). Much of the variability in the reported data for individual species may be due to the lack of normalization for specific respiratory parameters during exposure. In addition, the various studies have used different exposure techniques, such as nasal mask, oral mask, oral tube, or tracheal intubation. Regional deposition may be affected by the exposure route and delivery technique employed.

Figure 10-30 shows the regional deposition data versus particle diameter in commonly used laboratory animals obtained by various investigators and compiled by Schlesinger (1988). Although there is much variability in the data, it is possible to make some generalizations concerning comparative deposition patterns. The relationship between total respiratory tract deposition and particle size is approximately the same in humans and most of these animals; deposition increases on both sides of a minimum, which occurs for particles of 0.2 to 0.9 μm. Interspecies differences in regional deposition occur due to anatomical and

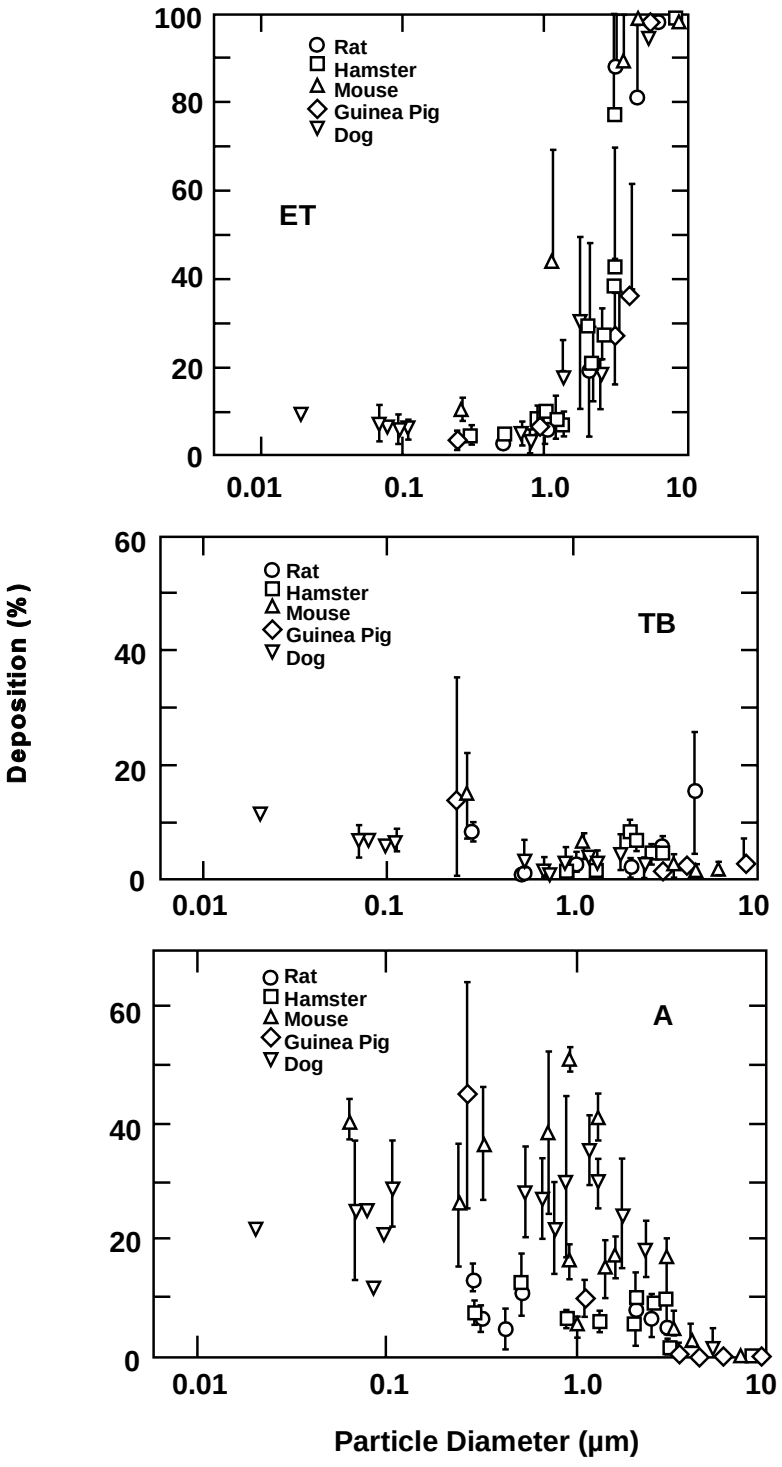

Figure 10-30. Regional deposition fraction in laboratory animals as a function of particle size. Particle diameters are aerodynamic (MMAD) for those > 0.5 μm and geometric (or diffusion equivalent) for those < 0.5 μm.

Source: Schlesinger (1988).

physiological factors. In most laboratory animal species, deposition in the ET region is near 100 percent for d_{ae} greater than 5 μm (Raabe et al., 1988), indicating greater efficiency than that seen in humans. In the TB region, there is a relatively constant, but lower, deposition fraction for d_{ae} greater than 1 μm in all species compared to humans. Finally, in the A region, deposition fraction peaks at a lower particle size (d_{ae} about 1 μm) in laboratory animals, than in humans.

Mathematical deposition models for rats, hamsters, and guinea pigs have been developed by several investigators (e.g., Schum and Yeh, 1980; Xu and Yu, 1987; Martonen et al., 1992) in a similar manner as the human models without including diffusion deposition in the ET region. Although the modeling results are generally in agreement with experimental data, there is a considerable uncertainty in the respiratory and anatomical parameters of the laboratory animals used in the modeling studies. In addition, the airway branching patterns in the animals are commonly monopodial as compared to the dichotomous branching in the human lung. The deposition efficiency of an airway (the amount of deposition in an airway divided by the amount entered) developed in the human model may not be applicable to laboratory animal species. Despite some of these difficulties, modeling studies in laboratory animals remain a useful step in extrapolating exposure-dose-response relationships from laboratory animals to the human (Yu et al., 1991).

Asgharian et al. (1995) developed an empirical model of particle deposition in the A region based on the published data reviewed by Schlesinger (1985a). Although restricted to the A region, the approach could be applied to other regions. A deposition function (F_A) was described using a polynomial regression of the form

$$F_A = \sum_{i=0}^{N} a_i(\log_{10} d)^i \text{ for } d \le d_{cut-off}, \text{ and} \quad (10\text{-}30)$$

$$F_A(d) = 0 \text{ for } d \ge d_{cut-off}. \quad (10\text{-}31)$$

where N = 4 is the degree of the polynomial, d is the particle diameter in micrometers, and $d_{cut-off}$ is the diameter at which the deposition efficiency becomes zero. Since Equation 10-30 is a 4^{th}-degree polynomial, it will give a non-zero value for $d_{cut-off}$. For this

reason, Equation 10-31 was added to be consistent with the deposition data and $d_{cut\text{-}off}$ was determined by setting Equation 10-30 to zero. Newton's method was employed to find $d_{cut\text{-}off}$ for different cases. Particle deposition was then integrated with particle distributions differing in median particle diameter and σ_g to calculate deposition mass fraction for specific polydisperse size distributions.

Ménache et al. (1996) developed an empirical model to estimate fractional regional deposition efficiency. This model represents a revised version of previously published models used for dosimetric interspecies extrapolation (Jarabek et al., 1989, 1990; Miller et al., 1988) that have been useful to develop inhalation reference concentration (RfC) estimates for dose-response assessment of air toxics (U.S. Environmental Protection Agency, 1994). For example, rather than linear interpolation between the published (Raabe et al., 1988) means for deposition measured at discrete particle diameters, as previously done for the rat deposition modeling, equations have now been fit to the individual animal data for each of the discrete, monodisperse particle exposures (U.S. Environmental Protection Agency, 1994; Ménache et al., 1996).

A description of the complete study including details of the exposure may be found elsewhere (Raabe et al., 1988). Briefly, the animals were exposed to radiolabelled ytterbium (^{169}Yb) fused aluminosilicate spheres in a nose-only exposure apparatus. Twenty unanesthetized rodents or eight rabbits were exposed to particles of aerodynamic diameters (d_{ae}) approximately 1, 3, 5, or 10 μm. Half the animals were sacrificed immediately post exposure; the remaining half were held 20 h post exposure. One-half of the animals at each time point were female. The animals were dissected into 15 tissue compartments, and radioactivity was counted in each compartment. The compartments included the head, larynx, GI tract, trachea, and the five lung lobes. This information was used directly in the calculation of the deposition fractions. Radioactivity was also measured in other tissues including heart, liver, kidneys, and carcass; and additionally in the urine and feces of a group of animals held 20 h. Data for the animals sacrificed immediately post exposure were used to ensure that there was no contamination of other tissue, whereas the data from the animals held 20 h were used in the calculation of a fraction used to partition bronchial deposition between the TB and A regions. Radioactivity was measured in the pelt, paws, tail, and headskin as a control on the exposure.

Although there are some other studies of particle deposition in laboratory animals (see review by Schlesinger, 1985a), no other data have the level of detail or the experimental design (i.e., freely breathing, unanesthetized, nose-only exposure to monodisperse particle size distributions) required to provide deposition equations representative of the animal exposures used in many inhalation toxicology studies. However, many inhalation toxicology studies are not nose-only exposures. While nose-only exposures are necessary to determine fractional particle deposition, adjustments can be made to estimate deposition fractions under whole-body exposure conditions. Similarly, deposition of polydisperse size distributions can be estimated by integrating the size distribution and monodisperse fractional deposition.

The advantages of using the data of Raabe et al. (1988) to develop the deposition efficiency equations include:

- the detailed measurements were made in all tissues in the animal, providing mass balance information and indicating that there was no contamination of nonrespiratory tract tissue with radioactivity immediately post exposure,

- the use of unanesthetized, freely breathing animals, and

- the use of monodisperse or near monodisperse particle size distributions in the exposures

Regional fractional deposition, F_r, was calculated as activity counted in a region normalized by total inhaled activity (Table 10-11). The proportionality factor, f_L, in Equations 10-33 and 10-34 was used to partition thoracic deposition between the TB and A regions. It was calculated using the 0 and 20-h data and is described in detail by Raabe and co-workers (1977).

These regional deposition fractions, F_r, however, are affected not only by the minute volume (V_E), MMAD and σ_g, but also by deposition in regions through which the particles have already passed. Deposition efficiency, η_r, on the other hand, is affected only by MMAD, σ_g and V_E. The relationships between deposition fraction and efficiency are calculated as provided below and are described in more detail elsewhere (Ménache et al., 1995). In the aerodynamic domain, that is for particles with diameters >0.5 μm, efficiencies increase monotonically and are bounded below by 0 and above by 1. The

TABLE 10-11. REGIONAL FRACTIONAL DEPOSITION

$$F_r = \frac{\text{Activity Counted in a Region}}{\text{Total Inhaled Activity}}$$

Extrathoracic (ET): $$F_{ET} = \frac{[\text{head} + \text{GI tract} + \text{larynx}]_{0\ h}}{\text{Total Inhaled Activity}} \quad (10\text{-}32)$$

Tracheobronchial (TB): $$F_{TB} = \frac{\text{trachea}_{0\ h} + f_L \times \sum_{i=1}^{5} \text{lobe}_{i,0\ h}}{\text{Total Inhaled Activity}} \quad (10\text{-}33)$$

Alveolar (A): $$F_A = \frac{(1 - f_L) \times \sum_{i=1}^{5} \text{lobe}_{i,0\ h}}{\text{Total Inhaled Activity}} \quad (10\text{-}34)$$

Source: U.S. Environmental Protection Agency (1994).

logistic function has mathematical properties that are consistent with the shape of the efficiency function (Miller et al., 1988)

$$E(\eta_r) = \frac{1}{1 + e^{\alpha + \beta \log_{10} x}}, \quad (10\text{-}35)$$

where $E(\eta_r)$ is the expected value of deposition efficiency (η_r) for region r, and x is expressed as an impaction parameter, $d_{ae}^2 Q$, for extrathoracic deposition efficiency and as aerodynamic particle size, d_{ae}, for TB and A deposition efficiencies. The flow rate, Q (mL/s), in the impaction parameter may be approximated by $(2V_E/60)$. The parameters α and β are estimated using nonlinear regression techniques.

To fit this model, efficiencies must be derived from the deposition fractions that were calculated as described in Table 10-11. Efficiency may be defined as activity counted in a region divided by activity entering that region. Then, considering the region as a sequence of filters in steady state, efficiencies may be calculated as follows

$$\eta_{ET} = F_{ET} \quad (10\text{-}36)$$

$$\eta_{TB} = \frac{\text{trachea}_{0\ h} + f_L \times \sum_{i=1}^{5} \text{lobe}_{i,0\ h}}{(1 - \eta_{ET})} \tag{10-37}$$

$$\eta_A = \frac{(1 - f_L) \times \sum_{i=1}^{5} \text{lobe}_{i,0\ h}}{(1 - \eta_{ET})\ (1 - \eta_{TB})}. \tag{10-38}$$

Using these calculated regional efficiencies in the individual animals, the logistic function was fit for the ET, TB, and A regions for the five animal species and humans. Figure 10-31 shows the deposition efficiency in the rat ET region versus the impaction parameter, d_{ae}^2Q. The logistic curve was fit to the experimental data assuming negligible deposition on exhalation. The open circles represent the data for animals having extreme studentized residuals (>1.96) compared to the data for other animals (closed circles) in the ET region. Deposition efficiency curves were fit for the TB and A regions also. In all three regions, the curve fits provided good descriptions of the data with asymptotic R^2 of 0.98 or greater (Ménache et al., 1996). The root MSE, an estimate of the average error in the regression model in the data units, ranged between 0.08 and 0.10. These differences are well within the limits of biological variability seen in this study and other studies (Schlesinger, 1988). The parameter estimates from these fits are listed in Table 10-12.

The fitted equations are then used to generate predicted efficiencies ($\hat{\eta}$) as a function of impaction in the ET region and of d_{ae} in the TB and A regions. Finally, the predicted efficiencies are multiplied together and adjusted for inhalability, I, as shown in Equations 10-39 through 10-41 to produce predicted deposition fractions ($\hat{F}_i$) for monodisperse and near monodisperse ($\sigma_g < 1.3$) particles

$$\hat{F}_{ET} = I \times \hat{\eta}_{ET} \tag{10-39}$$

$$\hat{F}_{TB} = I \times (1 - \hat{\eta}_{ET}) \times \hat{\eta}_{TB} \tag{10-40}$$

$$\hat{F}_A = I \times (1 - \hat{\eta}_{ET}) \times (1 - \hat{\eta}_{TB}) \times \hat{\eta}_A. \tag{10-41}$$

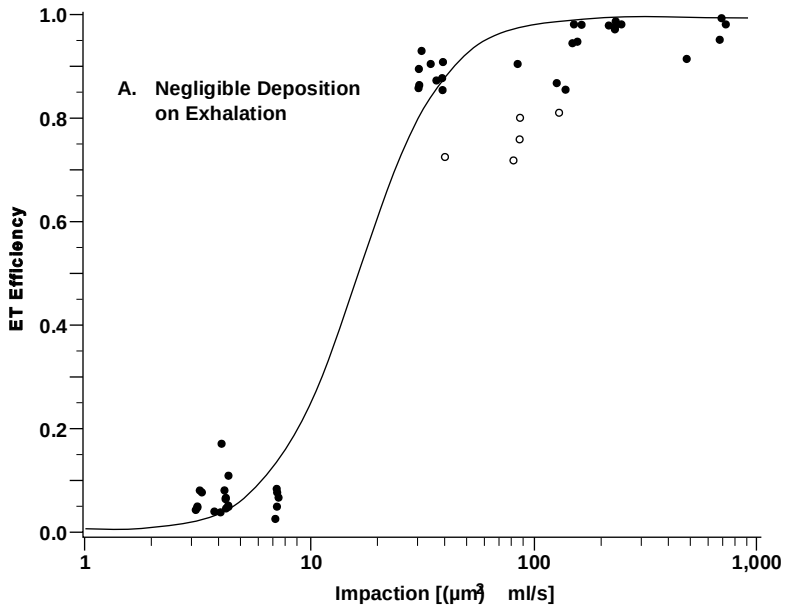

Figure 10-31. Regional deposition efficiency in the rat extrathoracic (ET) region versus an impaction parameter (d_{ae}^2Q) as predicted by model of Ménache et al. (1996).

Source: Ménache et al. (1996).

Inhalability, I, is an adjustment for the particles in an ambient exposure concentration that are not inhaled at all. For humans, an equation has been fit applying the logistic function (Ménache et al., 1995) to the experimental data of Breysse and Swift (1990)

$$I = 1 - \frac{1}{1 + e^{10.32 - 7.17 \log_{10} d_{ae}}} . \quad (10\text{-}42)$$

The logistic function was also fit to the data of Raabe et al. (1988) for laboratory animals (Ménache et al., 1995)

$$I = 1 - \frac{1}{1 + e^{2.57 - 2.81 \log_{10} d_{ae}}} . \quad (10\text{-}43)$$

Figure 10-32 illustrates the relationship between the predicted efficiencies and predicted depositions using this model for the rats. The particles were assumed to be monodisperse.

TABLE 10-12. DEPOSITION EFFICIENCY EQUATION ESTIMATED PARAMETERS AND 95% ASYMPTOTIC CONFIDENCE INTERVALS

	ET (Nasal)		TB		A	
Species	α	β	α	β	α	β
Human	7.129 [a]	-1.957[a]	3.298[a]	-4.588[a]	0.523[a]	-1.389[a]
Rat	6.348 (5.14, 7.56)	-5.269 (-6.19, -4.35)	2.822 (2.54, 3.11)	-4.576 (-5.06, -4.10)	2.241 (1.72, 2.77)	-10.463 (-12.74, -8.19)

[a]Source: Miller et al. (1988).

A default body weight (BW) for the rats of 0.38 kg was used to calculate a default $\dot{V}_E$ using allometric scaling (U.S. Environmental Protection Agency, 1994). Regional deposition efficiencies and fractions were calculated for particles with d_{ae} ranging from 1.0 to 10 μm. These calculated points were connected to produce the smooth curves shown in Figure 10-30. The three panels on the left of Figure 10-32 are plots of the predicted regional deposition efficiencies; the three panels on the right show the predicted regional deposition fractions derived from the estimated efficiencies and adjusted for inhalability. The vertical axis for the predicted deposition efficiency panels range from 0 to 1. Although the deposition fraction is also bounded by 0 and 1, the vertical axes in the figure are less than 1 in the TB and A regions. The top two panels of Figure 10-32 are the predicted deposition efficiency and fraction, respectively, for the ET region. These two curves are plotted as a function of the impaction parameter described for Equation 10-35. The middle two and lower two panels show the predicted deposition efficiencies and fractions for the TB and A regions, respectively. These four curves are plotted as a function of d_{ae}.

When a particle is from a monodisperse size distribution, the d_{ae} and the MMAD are the same. If, however, the particle is from a polydisperse size distribution, the particle cannot be described by a single d_{ae}; the average value of the distribution, the MMAD, must be used. In the aerodynamic particle size range, the deposition efficiency curves all increase monotonically as a function of the independent variable (i.e., either the impaction parameter or d_{ae}) and have both lower and upper asymptotes. The curves describing the deposition fractions, however, have different shapes that are dependent on the respiratory tract region. Deposition fractions in all three regions are nonmonotonic—initially increasing as a function of particle size but decreasing as particle sizes become larger. This is because particles that have been deposited in proximal regions are no longer available for deposition in distal regions. As an extreme example, if all particles are deposited in the ET region, no particles are available for deposition in either the TB or A regions. In the ET region, the nonmonotonic shape for fractional deposition is due to the fact that not all particles in an ambient concentration are inhalable.

As discussed in Section 10.2, particles in an experimental or ambient exposure are rarely all a single size but rather have some distribution in size around an average value.

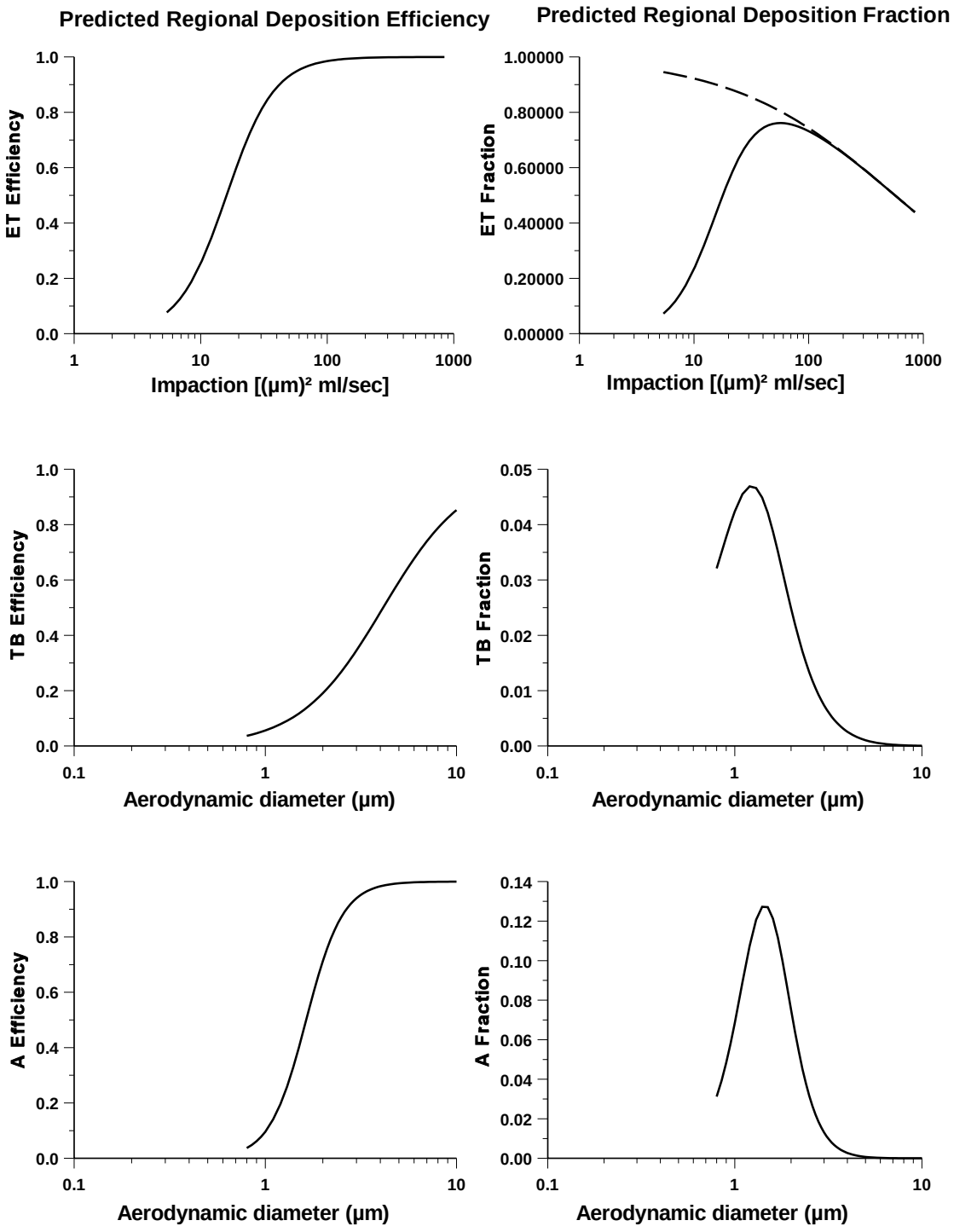

Figure 10-32. Comparison of regional deposition efficiencies and fractions for the rat. A default body weight of 0.38 kg (U.S. Environmental Protection Agency, 1994) was used in these calculations. The fractional deposition (solid line) and inhalability (dashed line) are shown in the upper right panel.

As this distribution becomes greater, the particle is said to be polydisperse. The empirical model of Ménache et al. (1996) was developed from exposures using essentially monodisperse particles (which are treated as though they are exactly monodisperse). It is therefore possible to multiply the particle size distribution function (which is customarily considered to be the lognormal distribution) by the predicted depositions (calculated as described in Equations 10-39 through 10-41) and integrate over the entire particle size range. Mathematically, this calculation is performed as described by Equation 10-44

$$[\hat{F}_r]_p = \int_0^{\infty} [\hat{F}_r]_m \times \frac{I}{d_{ae}(\log \sigma_g)\sqrt{2\pi}} \times \exp\left[-1/2\frac{(\log d_{ae} - \log MMAD)^2}{(\log \sigma_g)^2}\right] dd_{ae} , \quad (10\text{-}44)$$

where log refers to the natural logarithm, $[\hat{F}_r]_p$ is the predicted polydisperse fractional deposition for a given MMAD and σ_g, and $[\hat{F}_r]_m$ is the predicted monodisperse fractional deposition for particles of size d_{ae}. The limits of integration are defined from 0 to ∞ but actually include only four standard deviations (99.95% of the complete distribution). For each particle size in the integration, $[\hat{F}_r]_m$ is calculated and then multiplied by the probability of observing a particle of that size in a particle size distribution with that MMAD and σ_g. Rudolf and colleagues (1988) have also investigated the effect of polydisperse particle size distributions on predicted regional uptake of aerosols in humans and present a more detailed discussion of these and related issues.

As discussed by Schlesinger (1985a), there are many sources of variability that could explain differences in predicted deposition using the model of Ménache et al. (1996) and the observed deposition data in the studies reported by Schlesinger (1985a). However, results from the model of Asgharian et al. (1995), based on the data reported in Schlesinger (1985a), are similar to estimates derived using the model of Ménache et al. (1996).

Data from inhalation studies, particularly chronic inhalation exposures, are often difficult to interpret in terms of respiratory tract deposition efficiency, because the amounts of material retained in the respiratory tract and other body organs are often determined by complex relationships between initial lung deposition, lung retention, subsequent organ uptake and retention, and body uptake by ingestion of material contaminating the body surface. As an example, review of the literature indicates that data from most inhalation

deposition studies are not appropriate for direct comparison or model validation with the estimates from the Ménache et al. (1996) model because the data are normalized to the deposition in or on the animal rather than to what was inhaled (Newton and Pfledderer, 1986; Dahlbäck et al., 1989), used anesthetized animals (McMahon et al., 1977; Johnson and Ziemer, 1971; Raabe et al., 1977), or used cannulated animals (Shiotsuka et al., 1987). Berteau and Biermann (1977) exposed female Sprague Dawley rats to an aerosol with a mass median diameter (MMD) of 2.1 μm and a σ_g of 2.0 for 20 minutes. These authors calculated total deposition in 8 animals to be 28 ± 9.3%. The model of Ménache et al. (1996) would predict approximately 60% deposition, assuming the MMD = MMAD. Berteau and Biermann (1977) noted substantially lower deposition in rats than in mice for this same study and proposed a decrease in $\dot{V}_E$ as a possible reason. Some adjustment of $\dot{V}_E$ would bring the model prediction into closer agreement with the data. Differences in exposure such as whole-body and group housing versus nose-only could also contribute to some of the variability. Although there is substantial disagreement between the model prediction and the experimental measurement for this polydisperse aerosol, it seems likely that the experimental data are unusually low.

Dahlbäck and Eirefelt (1994) exposed male Sprague Dawley rats to monodisperse fluorescent polystyrene latex microspheres ranging in size from 0.63 to 5.7 μm count median diameter. Deposition was reported as the sum of nose, esophagus, stomach, and lung normalized to the amount deposited in the sum of these four compartments. Ménache et al. (1996) compared their model predictions with the experimental data for all particles > 1 μm. Because the experimental data were expressed as regional deposition normalized to total respiratory tract deposition, the model predictions were also normalized to total predicted respiratory tract deposition. To distinguish this presentation from presentation of deposition fractions elsewhere in this chapter, upper respiratory tract (URT) deposition is defined as the sum of the nose, esophagus, and stomach deposition divided by those three compartments plus the lung for the data of Dahlbäck and Eirefelt (1994); and as deposition in the ET region divided by deposition in the sum of the ET, TB, and A regions for the predictions using the Ménache et al. (1996). Lower respiratory tract (LRT) deposition may then be defined as

$$\text{LRT deposition} = 1 - \text{URT deposition}. \qquad (10\text{-}45)$$

The experimental and model-predicted deposition fractions are shown in Figure 10-33 for the data of Dahlbäck and Eirefelt (1994), as well as for the data of Raabe et al. (1988) that were used to develop the model. The solid line is the line of identity and represents the situation in which the predicted and observed deposition match exactly. As can be seen in Figure 10-33, there is considerable scatter in the data, particularly in the range associated generally with particles of about 2 to 3 μm MMAD. Under the conditions for which the model would predict 50 to 60 percent deposition, the observed deposition for both the URT and LRT ranges from 10 to 80 percent. As noted earlier (Figure 10-31) deposition in rats increases very rapidly from low to high values in this range. Similarly, in humans, regional deposition associated with particles of 2 to 3 μm ranges from 10 to 20 percent to 60 to 80 percent (Figure 10-22, 10-26, and 10-27).

10.6 CLEARANCE DATA AND MODELS

As discussed in previous sections, the biologic effects of inhaled particles are a function of their disposition. This, in turn, depends on their patterns of both deposition (i.e., the sites within which they initially come into contact with airway epithelial surfaces and the amount removed from the inhaled air at these sites) and clearance (i.e., the rates and routes by which deposited materials are removed from the respiratory tract). Removal of deposited materials involves the competing processes of macrophage - mediated clearance and dissolution - absorption. Deposition and clearance mechanisms were discussed in Sections 10.5 and 10.6, respectively.

Respiratory-tract clearance begins immediately upon deposition of inhaled particles. Given sufficient time, the deposited particles may be completely removed by these clearance processes. However, single inhalation exposures may be the exception rather than the rule. It is generally accepted that repeated or chronic exposures are common for environmental aerosols. As a result of such exposures, accumulations of the particles may occur. Chronic exposures produce respiratory tract burdens of inhaled particles that continue to increase with time until the rate of deposition is balanced by the rate of clearance. This is defined as the "equilibrium respiratory tract burden". The accumulation patterns are unique to each

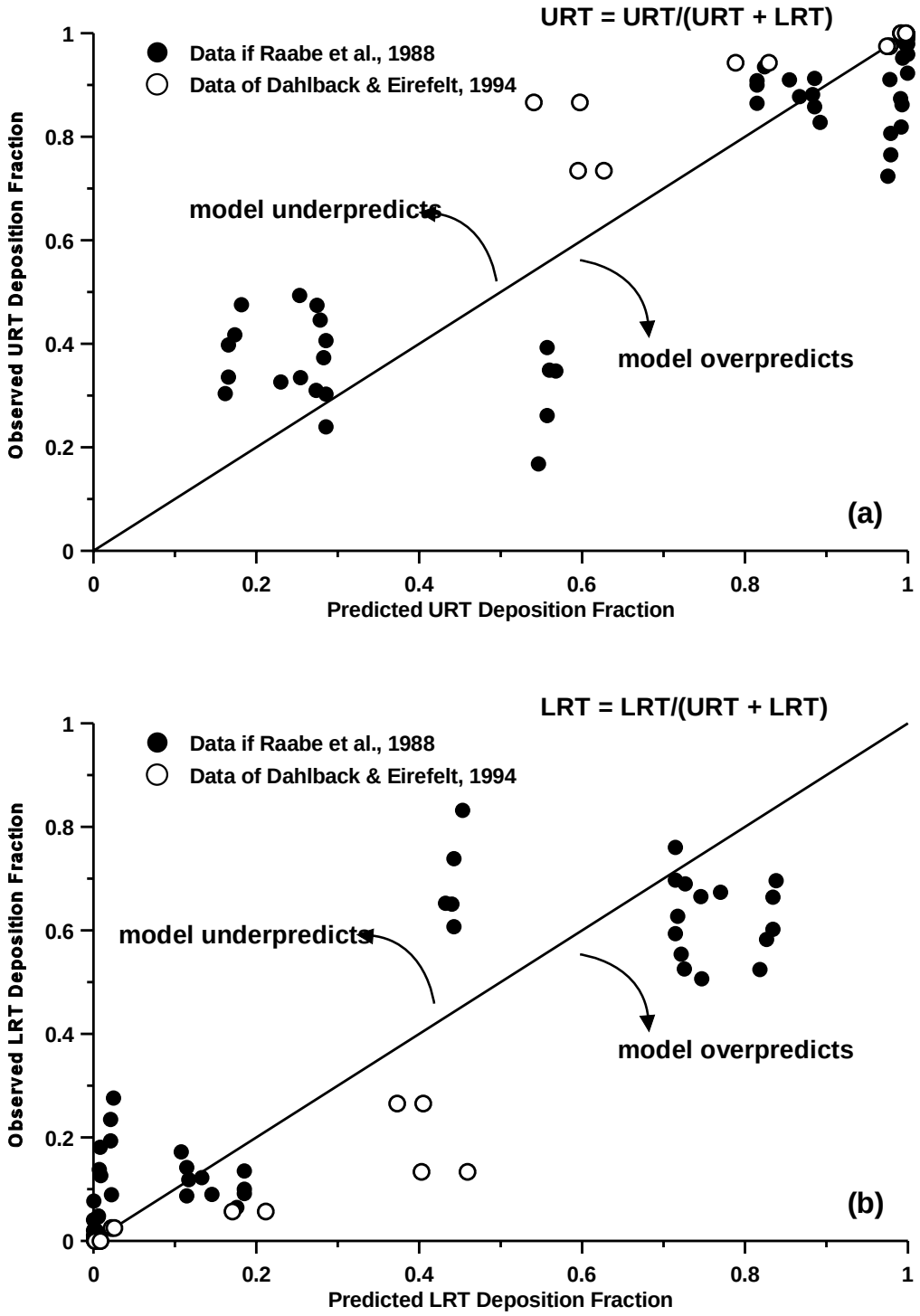

Figure 10-33. Experimental deposition fraction data and predicted estimates using model of Ménache et al. (1996). The solid line is the line of identity and represents the situation in which the predicted and observed deposition match exactly.

Source: Ménache et al. (1996).

laboratory animal species, and possibly unique to the inhaled material, especially if the inhaled material alters deposition and/or clearance patterns.

It is important to evaluate these accumulation patterns, especially when assessing ambient chronic exposures, because they dictate what the equilibrium respiratory tract burdens of inhaled particles will be for a specified exposure atmosphere. Equivalent concentrations can be defined as "species-dependent concentrations of airborne particles which, when chronically inhaled, produce equal lung deposits of inhaled particles per gram of lung during a specified exposure period". This section presents available data and approaches to evaluating exposure atmospheres that produce similar respiratory tract burdens in laboratory animals and humans.

10.6.1 Humans

Models for deposition, clearance, and dosimetry of the respiratory tract of humans have been available for the past four decades and continue to evolve. The International Commission on Radiological Protection (ICRP) has recommended three different mathematical models during this time period (ICRP 1959, 1979, 1994). The models changed substantially in structure, expanding from two compartments in the 1959 model (ICRP, 1959) to five compartments in the 1994 model (ICRP, 1994). These models have been an important aspect of radiation protection programs for inhaled radioactive materials. However, they make it possible to calculate the mass deposition and retention by different parts of the respiratory tract and provide, if needed, mathematical descriptions of the translocation of portions of the deposited material to other organs and tissues beyond the respiratory tract. The structure and complexity of the ICRP models increased with each version. These increases in complexity reflect both the expanded knowledge of the behavior and dosimetry of inhaled materials in the respiratory tract that has become available and an increased need for models that can be applied to a broader range of uses.

The 1959 model (ICRP, 1959) had a very simple structure in which the respiratory tract was divided into an upper respiratory tract (URT), and a lower respiratory tract (LRT). No information was given on the anatomical division between the URT and the LRT. In the 1959 model, 50% of inhaled particles deposited in the URT, 25% deposited in the LRT, and the remaining 25% was exhaled. No information on the effects of the sites or magnitude of

particle deposition was given, and relationships between particle size, deposition, and clearance were not incorporated into the 1959 model. The URT was considered an air passage from which all deposited particles cleared quickly by mucociliary activity and swallowed. Particles deposited in the LRT were classified as soluble or insoluble. For soluble particles, chemical constituents of all 25% of the inhaled particles that reach the LRT were assumed to be rapidly absorbed into the systemic circulation. For poorly soluble particles, 12.5% were assumed to clear by mucociliary activity and be swallowed during the first 24 h following deposition. The remaining 12.5% was assumed to be retained with a biological half-time of 120 d. No clearance of particles to the regional lymph nodes was included in the 1959 model.

The 1979 model (ICRP, 1979) was based on the Task Group Lung Model (TGLM) report (Morrow et al., 1966) and was divided into three compartments (nasopharyngeal, NP; tracheobronchial, TB; and pulmonary, PU). The NP region included anatomical structures from the tip of the nose to the larynx. The TB region extended from the trachea to the end of the terminal bronchioles. The PU region (equivalent to the A regional as described in Table 10-1) was the remaining, non-ciliated pulmonary parenchyma. Deposition probabilities were given for the NP, TB, and PU regions for activity median aerodynamic diameters (AMAD) of inhaled particles that covered about two orders of magnitude (0.2 - 10 μm). This incorporation of particle size considerations and the AMAD concept were major improvements in the health protection aspects of modeling related to inhaled radioactive particles. The 1979 ICRP model also incorporated consideration for clearance rates using three classes (D, W, Y). Class D particles cleared rapidly ($T_{1/2}$ = 0.5 d), class W particles cleared at an intermediate rate ($T_{1/2}$ = 50 d), and class Y particles cleared slowly ($T_{1/2}$ = 500 d). It was also recognized that the competing processes of dissolution-absorption and physical clearance operated on the deposited particles, but inadequate information was available to differentiate between the two mechanisms. This model also included a clearance pathway to the tracheobronchial lymph nodes. The long-term clearance of particles by either physical transport processes or by dissolution-absorption processes are described by the same clearance half-time.

A substantial increase in knowledge about the effects of particle size on the deposition of inhaled particles occurred since the publication of the TGLM report (Morrow et al.,

1966). This new information is reflected in the latest ICRP66 model (IRCP66, 1994). This new ICRP66 model considers the respiratory tract as four anatomical regions. The extrathoracic (ET) region is divided into two sub-regions: the anterior nasal airways, which clear only by extrinsic processes such as nose blowing, defined as ET_1, and the posterior nasal passages, pharynx, mouth and larynx defined as ET_2, which clears to the gastrointestinal tract via a combination of mucociliary action and fluid flow. The airways within the lungs are comprised of the bronchial (BB) and bronchiolar (bb) regions, which combined are equivalent to the Tracheobronchial (TB) region described in Table 10-3. The division of the TB region into two parts (bronchi and bronchiolar) by the ICRP enables mass deposition in the small airways to be evaluated separately, and possible related to such effects as small airways constriction. The gas-exchange tissues are defined as the alveolar-interstitial (AI) region, which is exactly comparable to the pulmonary region or A region (see Tables 10-1 and 10-3). There are two lymph node regions; LN_{ET} drains the extrathoracic region and LN_{TH} drains the BB, bb, and AI regions.

Deposition in the four anatomical regions (ET, BB, bb, and AI) is given as a function of particle size covering five orders of magnitude, and two different types of particle size parameters are used. The activity median thermodynamic diameter (AMTD) is used to describe the deposition of particles ranging in size from 0.0005 to 1.0 micrometer; the AMAD is used to describe deposition for the size range of 0.1 to 100 micrometer. The model applies to hygroscopic particles by estimating particle growth in each region during inhalation. Reference values of regional deposition are provided, and guidance is given for extrapolating to specific individuals and populations under different levels of activity. Deposition is expressed as a fraction of the number or activity of particles of a given size that is present in a volume of ambient air before inspiration, and activity is assumed to be log-normally distributed as a function of particle size for a typical particle density of 3 g/cm^3 and dynamic shape factor of 1.5, although particle density and shape factor are included as variables in the deposition calculations. As discussed in Section 10.5, the 1994 ICRP66 model also includes consideration of particle inhalability, which is a measure of the degree to which particles can enter the respiratory tract and be available for deposition.

After deposition occurs in a given region, two different clearance processes act competitively on the deposited particles, except in the ET_1 region where the only clearance

process is extrinsic. These processes are particle transport, which includes mucociliary clearance from the respiratory tract and physical clearance of particles to the regional lymph nodes, and absorption, which includes movement of material to blood including both dissolution-absorption and transport of ultra fine particles. Rates of particle clearance which were derived from studies with human subjects are assumed to be the same for all types of particles. Particle clearance from the BB and bb regions includes two slow phases: (1) to account for observations of slow mucociliary clearance in humans and (2) to account for observations of long term retention of small fractions of deposited material in the tracheobronchial tissues of both laboratory animals and humans. The structure for the ICRP66 1994 model is shown in Figure 10-34. A summary of the development of the ICRP66 1994 model is provided in Appendix 10A. This includes comparison of model predictions against the available depostion data discussed in Section 10.5.

A considerable amount of information has accumulated relevant to the biokinetics of inhaled radioactive materials. The radiation associated with these materials allows relative ease of analysis to determine temporal patterns for retention, distribution, and excretion of inhaled radioactive particles and their constituents. Non-radioactive particles are difficult to study because the particles and their chemical constituents are generally difficult to detect in biological systems, tissues, and excreta. Some studies have shown that the physicochemical forms and sites of deposition of chemical toxicants influence clearance rates. Also, adsorption of chemicals onto particles can influence deposition patterns and alter rates of dissolution-absorption of the particles and their constituents. For example, vapors that would not normally reach the A region will do so if they are adsorbed onto particles. Also, adsorption onto particles might slow the rates at which chemicals can be absorbed into lung tissue or the circulatory system. Amounts of inhaled material may markedly influence clearance as a consequence of particle overload. The cytotoxicity and shapes of particles (i.e., fibers) also influence clearance. Additionally, metabolic products of the inhaled materials may cause pathology and disease states that may result in nonpredictable retention and clearance patterns.

Absorption into blood is material specific, acts in all regions except ET_1, and is assumed to occur at the same rates for all regions. Absorption into blood is a two stage process. The first step (dissolution) involves dissociation of the particles into a form that can

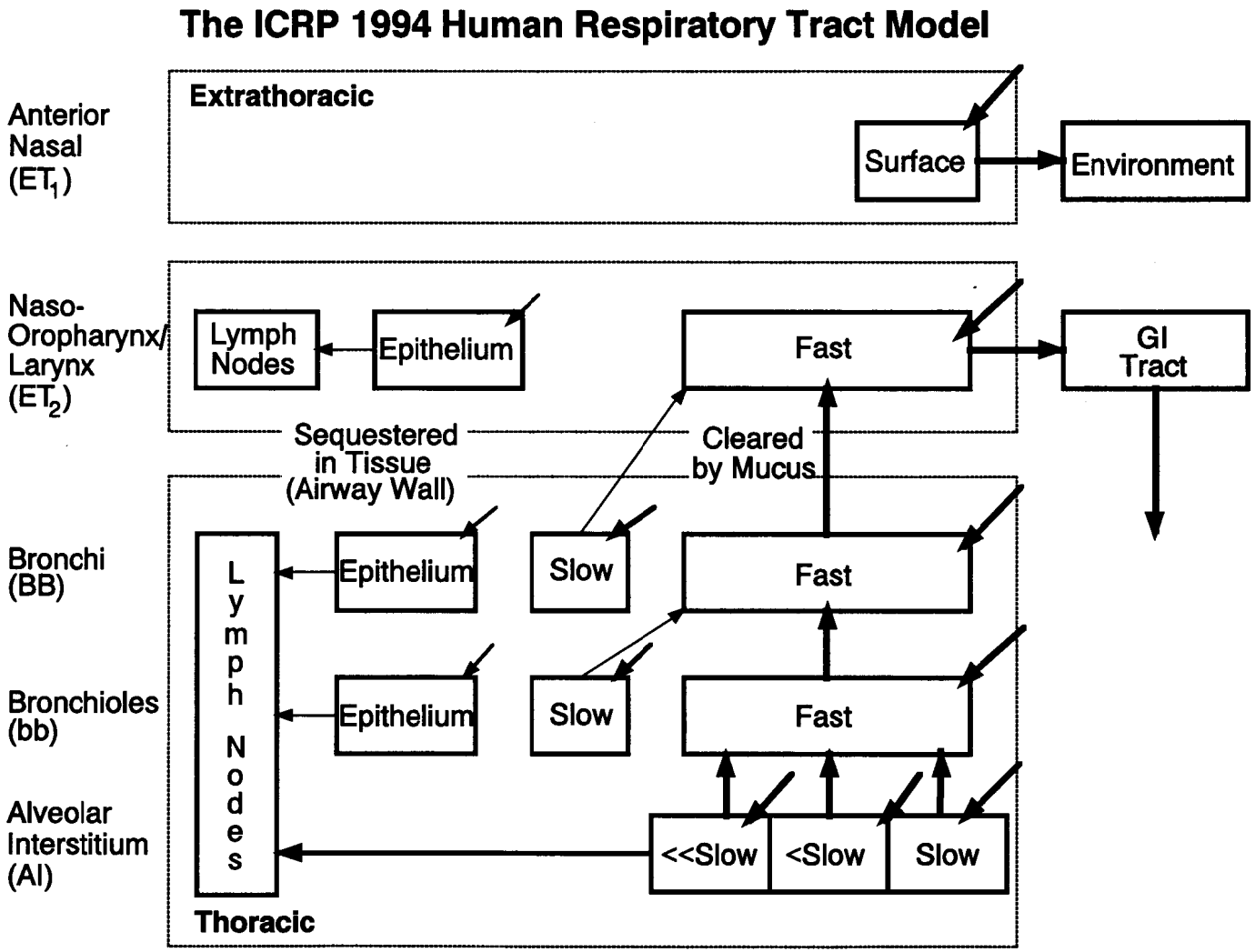

Figure 10-34. Schematic of the International Commission on Radiological Protection (ICRP66, 1994) model. Respiratory tract compartments in which inhaled particles may be deposited are illustrated. An explanation of clearance pathways, clearance rates, and subfractions of activity committed to different pathways is provided in the text.

Source: International Commission on Radiological Protection (ICRP66, 1994).

be absorbed into blood; the second step involves absorption of the subunits of the particles. Because these processes act independently on the regionally deposited particles, each can be specified separately and allowed to compete against the other processes involved in the model. This approach makes it possible to use time-dependent functions to describe processes such as dissolution-absorption. However, for ease of calculation it is assumed that time dependent dissolution can be approximated by dividing the material into two fractions with different dissolution rates: material in an initial state dissolves at a constant rate, simultaneously changing to a transformed state in which it dissolves at another rate. Uptake into blood is treated as instantaneous for the material immediately absorbed after dissolution. Another fraction of dissolved material may be absorbed more slowly as a result of binding with tissue components. The model can use observed rates of absorption for compounds for which there are reliable human or laboratory animal data. The absorption of other compounds are specified as fast, moderate or slow. In the absence of specific information, compounds are classified as fast, moderate or slow according to their former classification as D, W or Y, respectively, under the previous ICRP model. Greater attention to the transfer of particles to regional lymph nodes is given in this model than in the 1979 model by incorporating these clearance processes at each level in the respiratory tract, not just in the A or pulmonary region as in the 1979 model. Additionally, while the new ICRP66 model (ICRP66, 1994) was developed primarily for use with airborne radioactive particles and gases, its use for describing the dosimetry of inhaled mass of non-radioactive substances is also appropriate.

An alternative new respiratory tract dosimetry model that developed concurrently with the new ICRP model is being proposed by the National Council on Radiation Protection (NCRP). This model was described in outline by Phalen et al. (1991) and at the time of writing, a full report of the model is undergoing final approval by the NCRP. As with the 1994 ICRP66 model (ICRP66, 1994), the proposed NCRP model addresses (1) inhalability of particles, (2) new sub-regions of the respiratory tract, (3) dissolution-absorption as an important aspect of the model, and (4) body size (and age). The proposed NCRP model defines the respiratory tract in terms of a naso-oro-pharyngo-laryngeal (NOPL) region, a tracheobronchial (TB) region, a pulmonary (P) region, and the lung-associated lymph nodes (LN). As with the 1994 ICRP66 model, inhalability of aerosol particles is considered, and

deposition in the various regions of the respiratory tract is modeled using methods that relate to mechanisms of inertial impaction, sedimentation, and diffusion. The rates of dissolution-absorption of particles and their constituents are derived from clearance data from humans and laboratory animals. The effect of body growth on particle deposition is also considered in the model, but particle clearance rates are assumed to be independent of age. The NCRP model does not consider the fate of inhaled materials after they leave the respiratory tract. Although the proposed NCRP model describes respiratory tract deposition, clearance, and dosimetry for radioactive substances inhaled by humans, the model can also be used for evaluating inhalation exposures to all types of particles.

Both the NCRP and ICRP had the benefit of contributions from respected investigators in respiratory tract toxicology and biomedical aerosol research. Similar mathematical assessments were arrived at by both commissions, although detailed calculations for specific radionuclides can be different. Comparison of regional deposition fraction predictions between the two models are shown in Figures 10-35 through 10-37. As noted above, the various compartments of the two models are equivalent. That is, the ET region as described in Table 10-3 is equivalent to the ET_1 plus ET_2 compartments of the ICRP66 1944 model and the NOPL compartment of the proposed NCRP model. The TB region of Table 10-3 is equivalent to the BB plus bb compartments of the ICRP66 1994 model and to the TB compartment of the proposed NCRP model. The A region of Table 10-3 is equivalent to the AI compartment of the ICRP66 1994 model and to the P compartment of the proposed NCRP model. These differences in nomenclature are retained in these figures to aid distinguishing the predictions from each. Figures 10-35 and 10-36 show predictions for an adult male during mild exercise and at rest. Figure 10-37 shows predictions for a 5-year old child. These comparisons show that the behavior of the models are quite comparable, that is, the predicted deposition fraction for a given particle size is similar if the models use the same ventilation parameters as input. In fact, in order to insure a uniform course of action that provides a coherent and consistent international approach, the NCRP recommends adoption of the ICRP66 1994 model for calculating exposures for radiation workers and the public (e.g., for computing annual reference levels of intake and derived reference air concentrations).

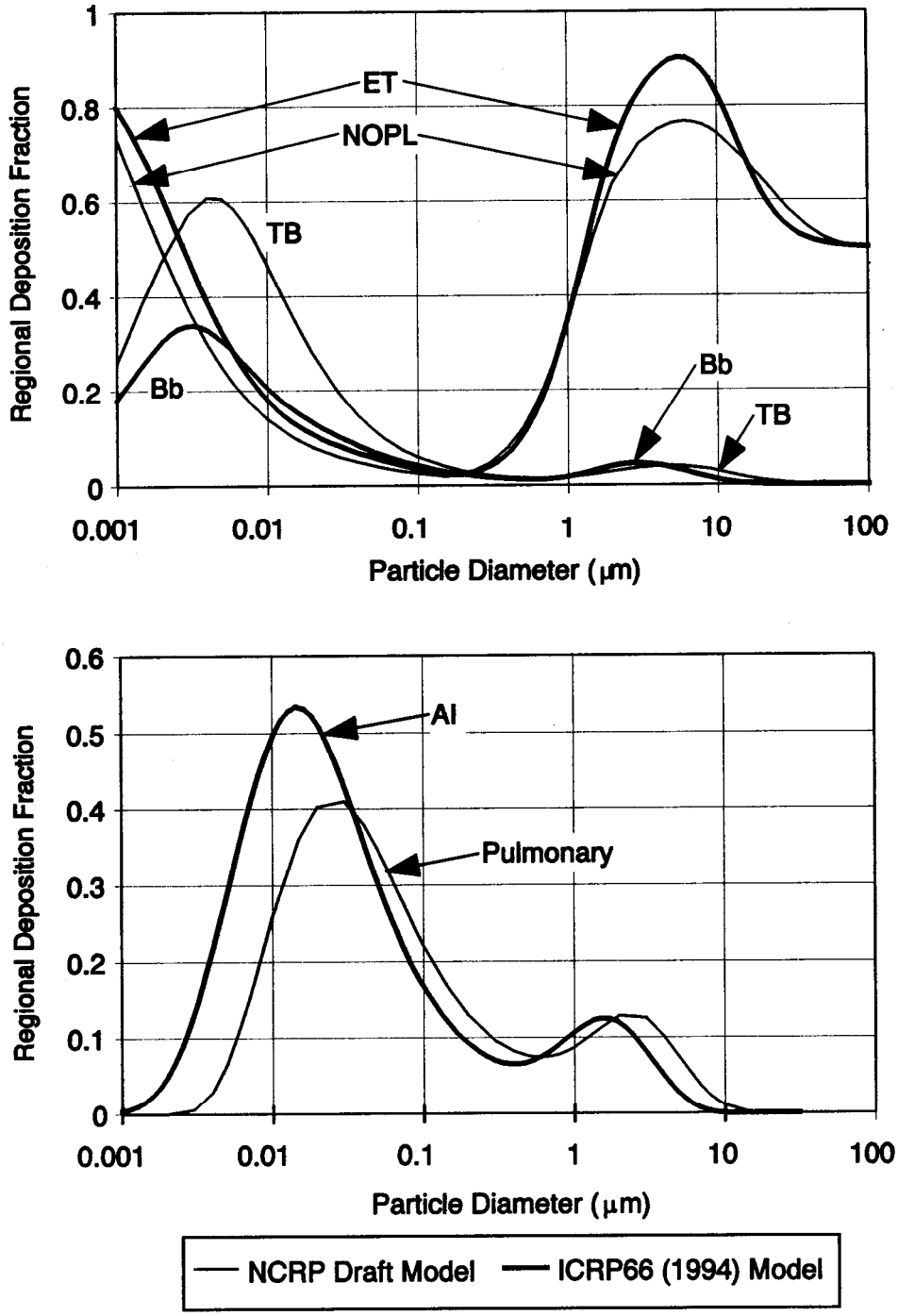

Figure 10-35. **Comparison of regional deposition fractions predicted by the proposed National Council on Radiation Protection (NCRP) model with those of the International Commission on Radiological Protection (ICRP) Publication 66 (1994) model. Predictions are for unit density, spherical particles inhaled through the nose by an adult male with a tidal volume of 1250 mL, respiratory frequency of 20 min^{-1}, and functional residual capacity (FRC) of 3300 mL. See text for an explanation of abbreviations for respiratory tract compartments.**

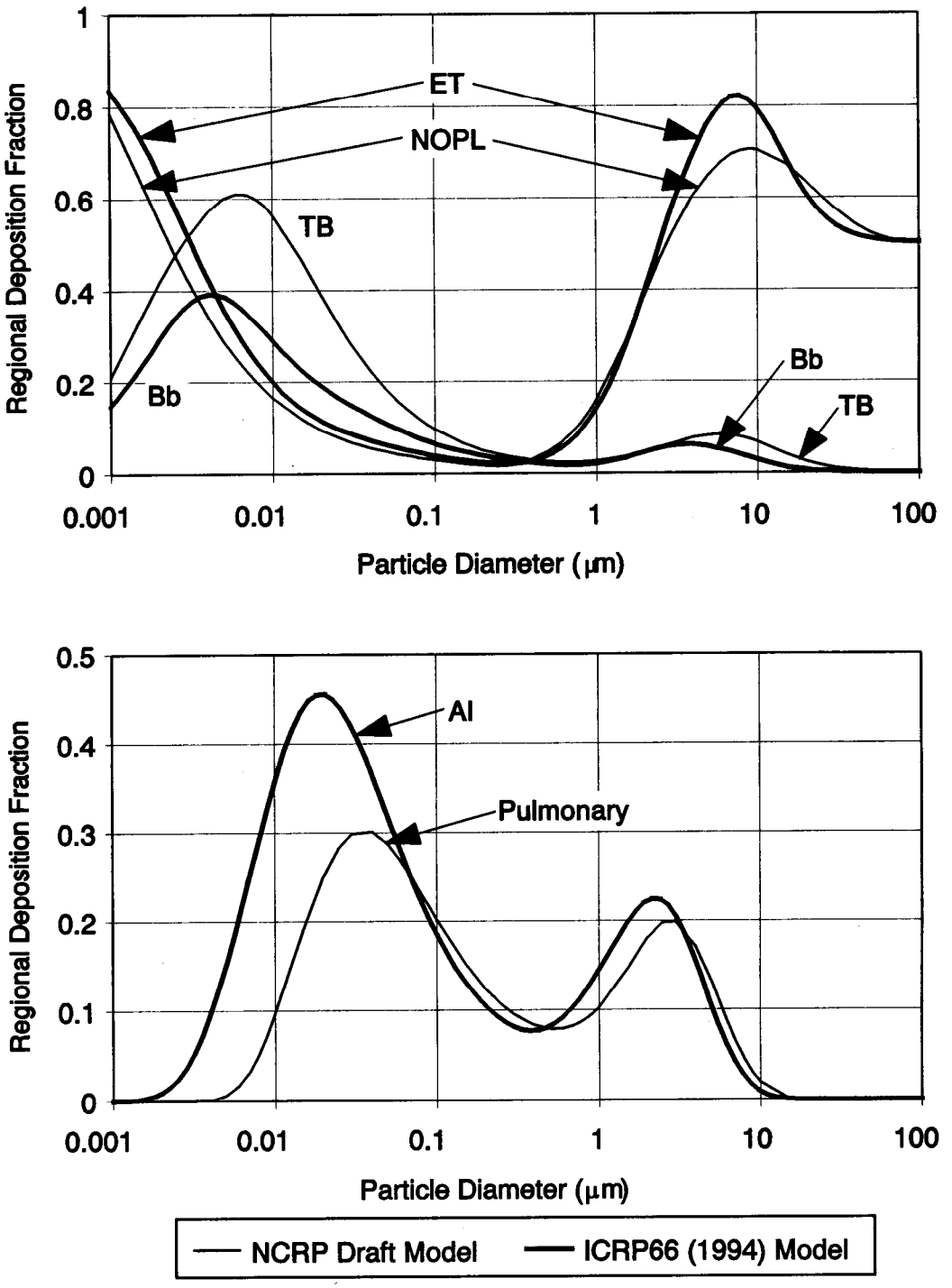

Figure 10-36. **Comparison of regional deposition fractions predicted by the proposed National Council on Radiation Protection (NCRP) model with those of the International Commission on Radiological Protection (ICRP) Publication 66 (1994) model. Predictions are for unit density, spherical particles inhaled through the nose by an adult male with a tidal volume of 750 mL, respiratory frequency of 12 min^{-1}, and functional residual capacity (FRC) of 3300 mL. See text for an explanation of abbreviations for respiratory tract compartments.**

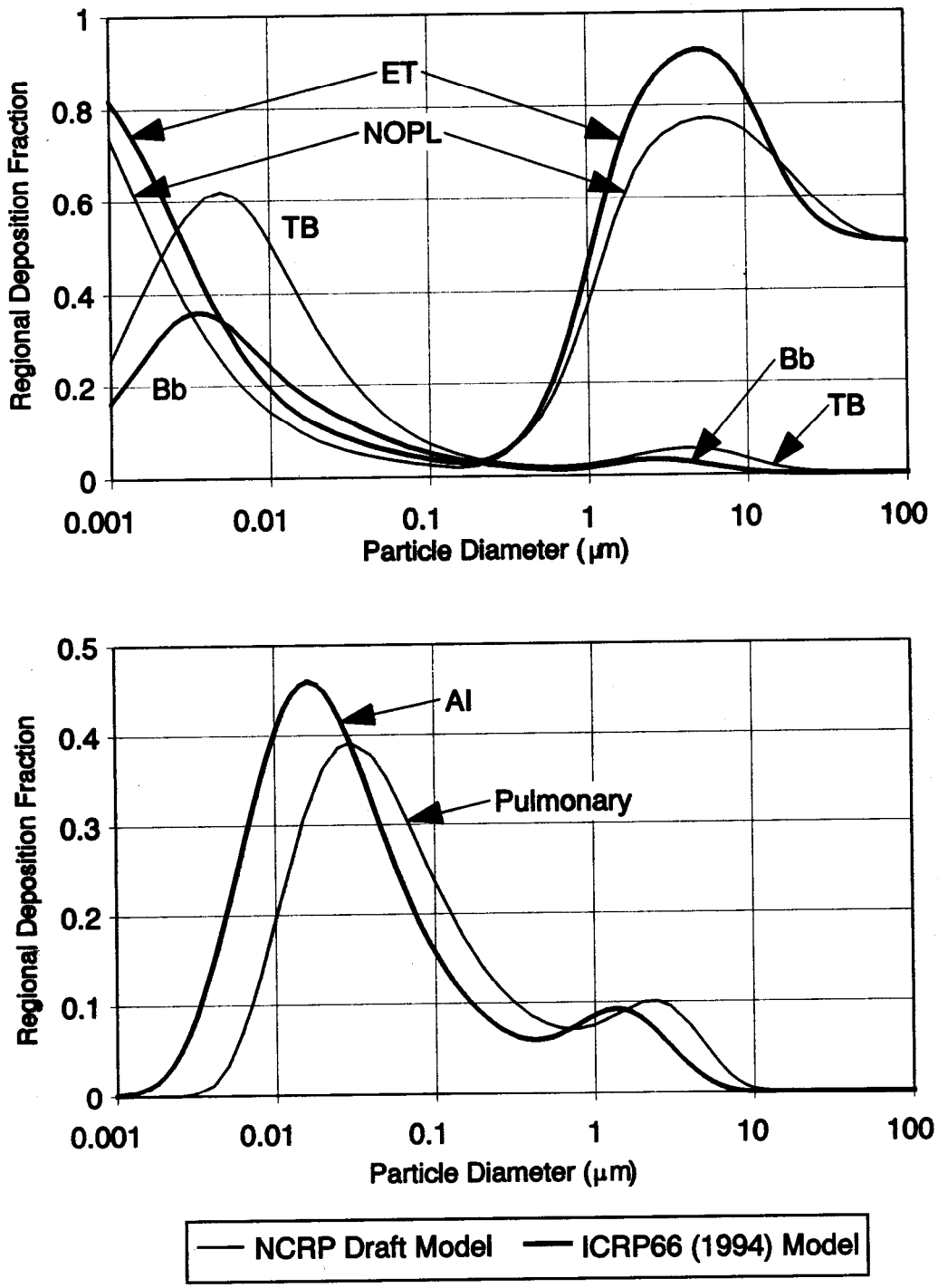

Figure 10-37. **Comparison of regional deposition fractions predicted by the proposed National Council on Radiation Protection (NCRP) model with those of the International Commission on Radiological Protection (ICRP) Publication 66 (1994) model. Predictions are for unit density, spherical particles inhaled through the nose by a 5-year-old child with a tidal volume of 244 mL, respiratory frequency of 39 min^{-1}, and functional residual capacity (FRC) of 767 mL. See text for an explanation of abbreviations for respiratory tract compartments.**

10.6.2 Laboratory Animals

Several laboratory animal models have been developed to help interpret results from specific studies that involved chronic inhalation exposures to non-radioactive particles (Wolff et al., 1987; Strom et al., 1988; Stöber et al., 1994). These models were adapted to data from studies involving high level chronic inhalation exposures in which massive lung burdens of low toxicity, poorly soluble particles were accumulated and the models have not been adapted to chronic exposures to low concentrations of aerosols in which particle overload does not occur.

Snipes et al. (1983) adapted a materials balance simulation model to evaluate repeated or chronic inhalation exposures. The simulation model language for a single inhalation exposure was described by Pritsker (1974) and uses a Fortran-based numerical integration of differential equations. The integration method is a fourth order, variable step-size Runge-Kutta-England routine for integrating systems of first order ordinary differential equations with initial values. The model was used to describe the retention and clearance of poorly soluble aerosol inhaled by mice, rats, and dogs (Snipes et al., 1983) and guinea pigs (Snipes et al., 1984). A distinct advantage of this kind of model is the requirement that dissolution-absorption rates for particles retained in the respiratory tract are approximated as part of the modeling process. The model output includes an estimate of the pulmonary burden of dust for each day of interest following an inhalation exposure.

Compartments and pathways of the model used in this chapter were kept as simple as necessary and were limited to those associated with the alveolar region of the respiratory tract. Figure 10-38 depicts the model, where

$D(t)$ = alveolar deposit of aerosol particles at time t (μg/g lung);

$MP(t)$ = mechanical transfer rate (fraction/day) for particles from the alveolar region to the mucociliary escalator for clearance to the gastrointestinal tract;

$ML(t)$ = mechanical transfer rate (fraction/day) for particles from the alveolar region to the thoracic lymph nodes;

$S(t)$ = dissolution-absorption rate (fraction/day) for particles in the alveolar region or thoracic lymph nodes.

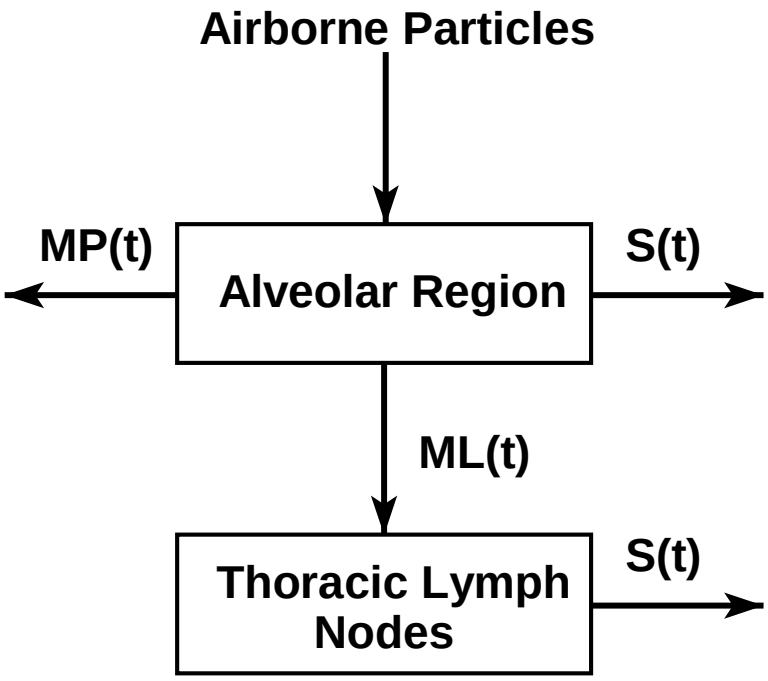

Figure 10-38. Compartments of the simulation model used to predict alveolar burdens of particles acutely inhaled by mice, hamsters, rats, guinea pigs, monkeys, and dogs. Definitions for parameters are provided in the text.

The retention of particles in the alveolar region as a function of time after a single inhalation exposure is described by

$$dD(t)/dt = -D(t) \cdot [MP(t) + ML(t) + S(t)], \quad (10\text{-}46)$$

with appropriate initial conditions for a single inhalation exposure. The solution of differential equations in the GASP IV simulation language is based upon numerical analysis techniques which adapt to produce solutions to a prespecified accuracy on either an absolute or relative scale. To maintain the specified accuracy the algorithm adjusts the size of the time step, making the step smaller or larger depending upon the estimated error. If the algorithm detects that the error is growing too large, it goes back to an earlier time and proceeds with smaller steps.

The simulation models for acute exposures were adapted to chronic exposures for the selected species using the assumption that each individual exposure during a chronic exposure

is the same with regard to deposition and clearance kinetics. Chronic exposures were simulated by defining the exposure duration in days and summing the amounts of dust retained in the lung from each daily inhalation exposure throughout the defined chronic exposure period. The model for chronic inhalation exposures therefore simply integrated the results of the individual exposures to predict the burdens of dust in the alveolar region during the course of the chronic exposures.

This model adequately accounted for the observed lung burdens of diesel exhaust particles (DEP) achieved in rats over the course of a 2-year chronic inhalation exposure to 0.35 mg DEP/m^3 (Snipes, 1989). The specific lung burdens of DEP achieved in the rats during the 2-year study were about 0.4 mg DEP/g lung, which is less that the amount that is generally predicted to cause particle overload. This model, and alternatives that are easily adapted to inhalation exposure scenarios, appears to be useful for predicting alveolar clearance patterns for a variety of inhaled materials as long as exposure concentrations are reasonably low and particle overload has not occurred.

10.6.3 Species Similarities and Differences

Rates for particle translocation from the A region to thoracic lymph nodes (TLNs) appear to vary considerably among species. Rats and mice have particle translocation rates from the A region to TLNs that are quite different from those of guinea pigs, dogs, and possibly humans (Snipes et al., 1983; 1984). Translocation from the A region to TLNs begins soon after an acute inhalation exposure. However, after a few days following the acute exposure, the transport of particles from the A region to TLNs appears to be negligible in mice and rats (Snipes et al., 1983), but continues at a constant rate in guinea pigs and dogs (Snipes et al., 1983; 1984). No experimental information is available about the rates of translocation of particles from the A region to TLNs in humans. However, data for amounts of particles accumulated in the lungs of humans exposed repeatedly to dusty environments (Stöber et al., 1967; Carlberg et al., 1971; McInroy et al., 1976; Cottier et al., 1987) suggest that poorly soluble particles accumulate in TLNs of humans at rates that may be comparable to those observed for guinea pigs, dogs, and monkeys. However, based on human autopsy data for particles found in thoracic lymph nodes and lung tissue, the ICRP (1994) determined a transport rate for particle from lung to lymph nodes that would result in

a lymph node/lung particle concentration ratio of 20 at 10,000 days after inhalation. The transport rate was 2×10^{-5}/day, i.e., lower than the rate for dogs and monkey by approximately a factor of ten.

Physical movement of particles from the A region to the TLNs affords the opportunity to transport particles out of the lung, but the result is to sequester, or trap the particles in what is generally perceived to be a dead-end compartment. Because the TLNs represent traps for particles cleared from the lung, particles can accumulate to high concentrations in the TLNs. Thomas (1968, 1972) discussed the implications of particle translocation from the A region to TLNs when the particles contain specific radionuclides, but he presented information that is relevant to all types of particles. Translocation of particles from the A region to the TLNs results in concentrations of particles in the lymph nodes that can be more than 2 orders of magnitude higher than concentrations in the lung. The implications of this consequence of inhalation exposures have not been fully evaluated but may have important implications for immunological responses in humans exposed to specific kinds of aerosols.

Many measurements of alveolar retention and clearance have been conducted on humans and a variety of laboratory animal species. In some cases, at least two laboratory animal species were exposed to the same aerosolized material, so direct comparisons among species are possible. Few human inhalation exposure studies have been performed using the same materials as used for the laboratory animal studies. Therefore, only a limited number of direct comparisons are possible between laboratory animals and humans.

Table 10-13 contains a summary of selected results for alveolar retention of inhaled materials after single inhalation exposures to small masses of poorly soluble particles. Studies of less than about 3 mo duration were not included. The variability in these results was caused by several factors. In many cases, the reported results did not allow division of the alveolar burden between short- and long-term clearance. Also, for most studies, dissolution-absorption of the exposure materials were not known or were not reported. The broad range of particle sizes would have influenced deposition patterns, and dissolution-absorption rates, but probably not physical clearance of particles from the A region. The alveolar burden as a function of time in days after acute inhalation is given by

TABLE 10-13. COMPARATIVE ALVEOLAR RETENTION PARAMETERS FOR POORLY SOLUBLE PARTICLES INHALED BY LABORATORY ANIMALS AND HUMANS

Species	Aerosol Matrix	Particle Size[a]		Alveolar Burden[b]				Study Duration (days)	References
		µm	Measure	P	T_1(d)	P_2	T_2(d)		
Mouse	FAP [c]	0.7	AMAD	[d] 0.93	34	0.07	146	850	Snipes et al. (1983)
	FAP	1.5	AMAD	0.93	35	0.07	171	850	Snipes et al. (1983)
	FAP	2.8	AMAD	0.93	36	0.07	201	850	Snipes et al. (1983)
	Ru oxide	0.38	CMD	0.88	28	[e] 0.12	230	490	Bair (1961)
	Pu oxide	0.2	CMD	0.86	20	0.14	460	525	Bair (1961)
Hamster	FAP	1.2	CMD	0.73	50	0.27	220	463	Bailey et al. (1985a)
Rat	Diesel soot	0.12	MMAD	0.37	6	0.63	80	330[f]	Lee et al. (1983)
	FAP	1.25	CMD	0.62	20	0.38	180	492	Bailey et al. (1985b)
	FAP	0.7	AMAD	0.91	34	0.09	173	850	Snipes et al. (1983)
	FAP	1.5	AMAD	0.91	35	0.09	210	850	Snipes et al. (1983)
	FAP	2.8	AMAD	0.91	36	0.09	258	850	Snipes et al. (1983)
	FAP	1.2	AMAD	0.83	33	0.17	310	365	Finch et al. (1994)
	FAP	1.4	AMAD	0.76	26	0.24	210	180	Finch et al. (1995)
	Asbestos fibers	1.2-2.3	AMAD			1.00	46-76	101-171	Morgan et al. (1977)
	Latex	3.0	CMD	0.39	18	0.61	63	190	Snipes et al. (1988)
	Pu oxide	<1.0	CMD	0.20	20	0.80	180	350	Langham (1956)
	Pu oxide	2.5	AMAD	0.75	30	0.25	250	800	Sanders et al. (1976)
	UO_2	2.7-3.2	AMAD			1.00	247	720	Morris et al. (1990)
	U_3O_8	≈1-2	CMD	0.67	20	0.33	500	768	Galibin and Parfenov (1971)
	Co_3O_4	2.69	MMAD	0.70	19	0.30	125	180	Kreyling et al. (1993)
Guinea pig	FAP	2.0	AMAD	0.22	29	0.78	385	1100	Snipes et al. (1984)
	Diesel soot	0.12	MMAD			1.00	>2,000	432	Lee et al. (1983)
	Latex	3.0	CMD			1.00	83	190	Snipes et al. (1988)

TABLE 10-13 (cont'd). COMPARATIVE ALVEOLAR RETENTION PARAMETERS FOR POORLY SOLUBLE PARTICLES INHALED BY LABORATORY ANIMALS AND HUMANS

Species	Aerosol Matrix	Particle Size		Alveolar Burden				Study Duration (days)	References
		µm	Measure	P	T_1(d)	P_2	T_2(d)		
Dog, (cont'd)	Coal dust	2.4	MMAD			1.00	1,000	160	Gibb et al. (1975)
	Coal dust	1.9	MMAD			1.00	≈700	301-392	Morrow and Yuile (1982)
	Ce oxide	0.09-1.4	MMD			1.00 [g]	>570	140	Stuart et al. (1964)
	FAP	2.1-2.3	AMAD	0.09	13	0.91	440	181	Boecker and McClellan, (1968)
	FAP	0.7	AMAD	0.15	20	0.85	257	850	Snipes et al. (1983)
	FAP	1.5	AMAD	0.15	21	0.85	341	850	Snipes et al. (1983)
	FAP	2.8	AMAD	0.15	21	0.85	485	850	Snipes et al. (1983)
	FAP	2.01	AMAD	0.05		0.95	910	1,000	Kreyling et al. (1988)
	Nb oxide	1.6 -2.5	AMAD			1.00	>300	128	Cuddihy (1978)
	Pu oxide	1-5	CMD			1.00	1,500	280	Bair (1961)
	Pu oxide	4.3	MMD			1.00	300	300	Bair et al. (1962)
	Pu oxide	1.1-4.9	MMAD		≈1		400	468	Morrow et al. (1967)
	Pu oxide	0.1-0.65	CMD	0.10	200	0.90	1,000	≈4,000	Park et al. (1972)
	Pu oxide	0.72	AMAD	0.10	3.9	0.90	680	730	Guilmette et al. (1984)
	Pu oxide	1.4	AMAD	0.32	87	0.68	1,400	730	Guilmette et al. (1984)
	Pu oxide	2.8	AMAD	0.22	32	0.78	1,800	730	Guilmette et al. (1984)
	Pu oxide	4.3	MMD	0.50	20	0.50	1,600	270	Bair and McClanahan (1961)
	Tantalum	4.0	AMAD	0.40	1.9	0.60	860	155	Bianco et al. (1974)
	U_3O_8	0.3	CMD	0.47	4.5	0.53	120	127	Fish (1961)
	Zr oxide	2.0	AMAD			1.0	340	128	Waligora (1971)
Monkey	Pu oxide	2.06	CMAD			1.0	500-900	200	Nolibe et al. (1977)
	Pu oxide	1.6	AMAD			1.0	770-1,100	990	LaBauve et al. (1980)
Human	FAP	1	CMD	0.14	40	0.86	350	372-533	Bailey et al. (1985a)
	FAP	4	CMD	0.27	50	0.73	670	372-533	Bailey et al. (1985a)

TABLE 10-13 (cont'd). COMPARATIVE ALVEOLAR RETENTION PARAMETERS FOR POORLY SOLUBLE PARTICLES INHALED BY LABORATORY ANIMALS AND HUMANS

Species	Aerosol Matrix	Particle Size		Alveolar Burden				[b] Study Duration (days)	References
		µm	Measure	P	T_1(d)	P_2	T_2(d)		
Human, (cont'd)	Latex	3.6	CMD	0.27	30	0.73	296	≈480	Bohning et al. (1982)
	Latex	5	CMD	0.42	0.5	0.58	150-300	160	Booker et al. (1967)
	Pu oxide	0.3	MMD			1.00	240	300	Johnson et al. (1972)
	Graphite and PuO_2	6	AMAD			1.00	240-290	566	Ramsden et al. (1970)
	Pu oxide	<4-5	CMD			1.00	1,000	427	Newton (1968)
	Th oxide	<4-5	CMD			1.00	300-400	427	Newton (1968)
	Teflon	4.1	CMD	0.30	4.5-45	0.70	200-2,500	300	Philipson et al. (1985)
	Zr oxide	2.0	AMAD			1.00	224	261	Waligora (1971)

[a]Some aerosols were monodisperse, but most were polydisperse, with geometric standard deviations in the range of 1.5 to 4.

[b]Alveolar burden = $P_1 \cdot e^{-(\ln 2)t/T_1} + P_2 \cdot e^{-(\ln 2)t/T_2}$, where P_1 and P_2 are fractions constrained to total 1.00, T_1 and T_2 equal retention half-times in (d), and t equals days after exposure. Retention half-times are approximations and are the net result of dissolution-absorption and physical clearance processes. In some examples, the original data were subjected to a computer curve-fit procedure to derive the values for P_1 and T_1 presented in this table.

[c]FAP = fused aluminosilicate particles.

[d]AMAD = activity median aerodynamic diameter.

[e]CMD = count median diameter.

[f]MMAD = mass median aerodynamic diameter.

[g]MMD = mass median diameter.

$$P_1 \cdot e^{-(\ln 2)t/T_1} + P_2 \cdot e^{-(\ln 2)t/T2}, \quad (10\text{-}47)$$

where P_1 and P_2 are fractions constrained to total 1.0, T_1 and T_2 equal retention half-times in days, and t equals days after acute exposure.

The information shown in Table 10-13 was used to approximate biological clearance rates for particles inhaled by the species listed in Table 10-14. In addition, approximations are included for the fractions of alveolar burdens initially deposited in the A region that were subjected to short- or long-term clearance. These trends clearly will not apply to all types of inhaled particles. For example, in some cases, deposition and clearance may be influenced by the physicochemical and/or biological characteristics of the inhaled material. Further, the generalizations that led to Table 10-14 allow comparisons for the consequences of chronic inhalation exposures among these animal species and humans that might not otherwise be possible.

TABLE 10-14. AVERAGE ALVEOLAR RETENTION PARAMETERS FOR POORLY SOLUBLE PARTICLES INHALED BY SELECTED LABORATORY ANIMAL SPECIES AND HUMANS

	Alveolar Retention Parameters[a]			
Species	**P_1**	**T_1**	**P_2**	**T_2**
Mouse	**0.9**	**30**	**0.1**	**240**
Rat, Syrian hamster	**0.9**	**25**	**0.1**	**210**
Guinea pig	**0.2**	**29**	**0.8**	**570**
Monkey, dog, human	**0.3**	**30**	**0.7**	**700**

[a]Alveolar burden (fraction of initial deposition) =

$$P_1 \exp^{(-\ln 2)t/T}1 + P_2 \exp^{(-\ln 2)t/T}2,$$

where:

P_1 and P_2 = fractions of alveolar burden in fast and slow-clearing components;
T_1 and T_2 = retention half-times (days) for P_1 and P_2; and
t = time in days after an acute inhalation exposure.

The mathematical expressions for fitting curves to data are dependent on the study duration. The values for percent initial alveolar burden (% IAB) versus time in the following table were obtained by simulating alveolar retention of poorly soluble particles in the rat using the physical clearance rates from Table 10-14. Two-component exponential curves were next fit for % IAB versus time using the model results for days 1 to 150, 1 to 300, and 1 to 730. As indicated in Table 10-15, the curve fitting parameters for the data for days 1 to 150 agree well with results typically seen in relatively short-term alveolar clearance studies with rats.

TABLE 10-15. PHYSICAL CLEARANCE RATES

Days	% IAB	P_1	T_1	P_2	T_2
1	96.96				
7	81.21				
14	66.89				
28	47.00				
35	40.03				
42	34.43				
49	29.87				
56	26.14				
63	23.06				
70	20.49				
100	13.26				
150	7.80	71.6	18.4	29.4	78.3
200	5.39				
250	4.10				
300	3.30	84.4	22.0	15.6	131
400	2.36				
500	1.78				
600	1.37				
730	0.99	91.0	25.6	9.0	221

Physical clearance patterns for alveolar burdens of particles are similar for guinea pigs, monkeys, dogs, and humans. For these species, about 20 to 30% of the initial burden of particles clears with a half-time on the order of 1 mo, the balance clears with a half-time of several hundred days. Mice, Syrian hamsters, and rats clear about 90% of the deposited

particles with a half-time of about 1 month and 10% with a half-time greater than 100 days. The relative division of the alveolar burden between short-term and long-term clearance represents a significant difference between most rodents and larger mammals and has considerable impact on long-term patterns for retention of material acutely inhaled, as well as for accumulation patterns for materials inhaled in repeated exposures.

10.6.4 Models To Estimate Retained Dose

Models have routinely been used to express retained dose in terms of temporal patterns for alveolar retention of acutely inhaled materials. Available information for a variety of mammalian species and humans can be used to predict deposition patterns in the respiratory tract for inhalable aerosols with reasonable degrees of accuracy. Additionally, as indicated above, alveolar clearance data for mammalian species commonly used in inhalation studies are available from numerous experiments that involved small amounts of inhaled radioactive particles. The amounts of particles inhaled in those studies were small and can be presumed to result in clearance patterns characteristic of the species unless radiation damage was a confounding factor, which was probably not the case except where acute effects were an experimental objective.

A very important factor in using models to predict retention patterns in laboratory animals or humans is the dissolution-absorption rate of the inhaled material. Factors that affect the dissolution of materials or the leaching of their constituents in physiological fluids, and the subsequent absorption of these constituents, are not fully understood. Solubility is known to be influenced by the surface-to-volume ratio and other surface properties of particles (Mercer, 1967; Morrow, 1973). The rates at which dissolution and absorption processes occur are influenced by factors that include chemical composition of the material. Temperature history of materials is an important consideration for some metal oxides. For example, in controlled laboratory environments, the solubility of oxides usually decreases when the oxides are produced at high temperatures, which generally results in compact particles having small surface-to-volume ratios. It is sometimes possible to accurately predict dissolution-absorption characteristics of materials based on physical/chemical considerations. However, predictions for *in vivo* dissolution-absorption rates for most materials, especially if they contain multivalent cations or anions, should be confirmed experimentally.

Phagocytic cells, primarily macrophages, clearly play a role in dissolution-absorption of particles retained in the respiratory tract (Kreyling, 1992). Some particles dissolve within the phagosomes due to the acidic milieu in those organelles (Lundborg et al., 1984, 1985), but the dissolved material may remain associated with the phagosomes or other organelles in the macrophage rather than diffuse out of the macrophage to be absorbed and transported elsewhere (Cuddihy, 1984). Examples of delayed absorption of presumably soluble inorganic materials are beryllium (Reeves and Vorwald, 1967) and americium (Mewhinney and Griffith, 1983). This same phenomenon has been reported for organic materials. For example, covalent binding of benzo(a)pyrene or metabolites to cellular macromolecules resulted in an increased alveolar retention time for that compound after inhalation exposures of rats (Medinsky and Kampcik, 1985). Certain chemical dyes are also retained in the lung (Medinsky et al., 1986), where they may dissolve and become associated with lipids or react with other constituents of lung tissue. Understanding these phenomena and recognizing species similarities and differences are important for evaluating alveolar retention and clearance processes and interpreting results of inhalation studies.

In one study related to the issue of species differences in dissolution-absorption, Oberdörster et al. (1987) evaluated clearance of ^{109}Cd from the lungs of rats and monkeys after inhalation of ^{109}Cd-labeled aerosols of $CdCl_2$ and CdO. The inhaled Cd was cleared 10 times faster from lungs of the rats than from the lungs of monkeys. Cadmium in the lungs of mammalian species is probably bound to metallothionein, and these differences in rates of Cd clearance appear to be the result of species differences in metallothionein metabolism. Bailey et al. (1989) conducted a study that included an interspecies comparison of the translocation of ^{57}Co from the A region to blood after inhalation of $^{57}Co_3O_4$. The results of this multi-species study suggest that mammalian species demonstrate considerable variability with regard to rates of dissolution of particles retained in lung tissue, degree of binding of solubilized materials with constituents of lung tissue, and rates of absorption into the circulatory system.

Dissolution-absorption of materials in the respiratory tract is clearly dependent on the chemical and physical attributes of the material. While it is possible to predict rates of dissolution-absorption, it is prudent to experimentally determine this important clearance parameter to understand the importance of this clearance process for the lung, TLNs,

and other body organs that might receive particles or fibers, or their constituents which enter the circulatory system from the lung.

10.6.4.1 Extrathoracic and Conducting Airways

Insufficient data are available to adequately model long-term retention of particles deposited in the conducting airways of any mammalian species. It is probable that some particles that deposit in the airways of the head and TB region during an inhalation exposure are retained for long times and may represent significant dosimetry concerns. Additionally, some of the particles that are cleared from the A region via the mucociliary transport pathway may become trapped in the TB epithelium during their transit through the airways. Additional research must be done to provide the information needed to properly evaluate retention of particles in conducting airways.

Based on the results of longitudinal studies of dogs who inhaled promethium oxide particles, Stuart (1966) concluded that some particles were retained for relatively long times in the heads. A study by Snipes et al. (1983) included mice, rats, and dogs exposed by inhalation to monodisperse or polydisperse ^{134}Cs-labeled fused aluminosilicate particles. In all three species, 0.001 to 1% of the initial internally deposited burden of particles was retained in the head airways and was removed only by dissolution-absorption. Tissue autoradiography revealed that retained particles were in close proximity to the basement membrane of nasal airway epithelium. In another study by Snipes et al. (1988), 3-, 9-, and 15-µm latex microspheres were inhaled by rats and guinea pigs. About 1 and 0.1% of all three sizes of microspheres were retained in the head airways of the rats and guinea pigs, respectively. For rats, the 9- and 15-µm microspheres cleared with half-times of 23 days; for guinea pigs, microspheres of this size cleared with half-times of about 9 days. The 3-µm microspheres were cleared from the head airways of the rats and guinea pigs with biological half-times of 173 and 346 days, respectively. The smaller particles are apparently more likely to penetrate the epithelium and reach long-term retention sites.

Whaley et al. (1986) studied retention and clearance of radiolabeled, 3-µm polystyrene latex particles instilled onto the epithelium of the maxillary and ethmoid turbinates of Beagle dogs. Retention of the particles at both sites after 30 days was about 0.1% of the amount

initially deposited. Autoradiographs of turbinate tissue indicated that the particles were retained in the epithelial submucosa of both regions.

It is also generally concluded that most inhaled particles that deposit in the TB region clear within hours or days. However, results from a number of studies in recent years challenge this supposition. These studies have demonstrated that small portions of the particles that deposit in, or are cleared through, the TB region are retained with half-times on the order of weeks or months. Patrick and Stirling (1977) noted that about 1% of barium sulfate particles instilled intratracheally into rats remained in the bronchial tissue for at least 30 days. In a followup study, Stirling and Patrick (1980) used autoradiography to demonstrate the temporal retention patterns for some of the retained $^{133}BaSO_4$ particles in TB airways. The particles were retained within macrophages in the tracheal wall for at least 7 days after intratracheal instillation of $^{133}BaSO_4$. By two h after instillation, some of the particles were buried in the tracheal wall. After 24 h, when most of the initial deposition of particles had cleared, 74% of $^{133}BaSO_4$ particles located by autoradiography were in macrophages proximate to the basement membrane. After 7 days, practically all of the remaining particles were incorporated into the walls of the airways. The authors did not determine the mechanisms by which the particles were moved into the airway epithelium. It is possible that the particles were phagocytized by macrophages and transported into the airway epithelium. Another possibility is direct uptake by epithelial cells of the airways. It is also probable that intratracheal instillation procedures perturb airway epithelium and influence the results of these kinds of studies.

Gore and Thorne (1977) exposed rats by inhalation to polydisperse aerosols of UO_2. At 2, 4, 7, and 35 days after inhalation of the UO_2, autoradiography was used to determine the locations of particles retained in the TB and A regions. The authors did not report seeing particles of UO_2 retained in the airways, but did note two phases of clearance. The first phase was associated with a clearance half-time of 1.4 days, the second phase with a clearance half-time of about 16 days. The faster clearance was presumably associated with particles deposited on the conducting airways during the inhalation exposure; the longer-term clearance was associated with clearance of UO_2 particles from the A region. In a separate study, Gore and Patrick (1978) evaluated the distribution of UO_2 particles in the trachea and bronchi of rats for up to 14 days after inhalation of aerosols similar to those used by Gore

and Thorne (1977). Retention of UO_2 at airway bifurcations was noted, as was retention of particles in the trachea.

In another study, Gore and Patrick (1982) also compared the retention sites of inhaled UO_2 particles and intratracheally instilled barium sulphate particles. Both types of particles were found in macrophages at sites near the basement membrane of the airways of the TB region. The macrophages appeared to have engulfed the particles in the airways, then passed through the airway epithelium and remained in the vicinity of the basement membrane. About 4% of the UO_2 in lungs of rats was associated with intrapulmonary airways (Gore, 1983; Patrick, 1983). Watson and Brain (1979) observed similar results with aerosols of gold colloid and iron oxide. Both types of particles were found in bronchial epithelium, but more of the iron oxide was observed, suggesting a possible particle size effect, or a relationship between the process of material uptake and chemical composition of the material. Both types of particles were found in bronchial epithelial cells, but neither gold nor iron oxide particles were seen in interstitial macrophages.

In another inhalation study, Briant and Sanders (1987) exposed rats to 0.7 μm AMAD chain-aggregate aerosols of U-Pu. These authors observed retained particles of U-Pu in the larynx, trachea, carina, and bronchial airways throughout the course of their 84-day study. The amounts retained varied, but were at any time approximately 1% of the concurrent alveolar burden. The alveolar burden of U-Pu cleared with a biological half-time of 100 days, and the relative amounts of U-Pu in the airways suggested comparable particle clearance rates from the airways. Particles of U-Pu retained in the airways were located in epithelial cells.

Stahlhofen et al. (1981, 1986) conducted inhalation studies with humans to directly assess deposition and retention of poorly soluble particles that deposit in the TB region by inhalation. Human subjects inhaled small volumes of aerosols using procedures that theoretically allowed deposition to occur at specific depths in the TB region, but not in the A region. Results of those studies suggested that as much as 50% of the particles that deposited in the TB region clear slowly, presumably because they become incorporated into the airway epithelium. Smaldone et al. (1988) reported the results from gamma camera imaging analyses of aerosol retention in normal and diseased human subjects, and also suggested that particles deposited on central airways of the human lung do not completely

clear within 24 h. There have also been a few reports indicating that poorly soluble particles associated with cigarette smoke are retained in the epithelium of the tracheobronchial tree of humans (Little et al., 1965; Radford and Martell, 1977; Cohen et al., 1988). The cumulative results of these studies strongly suggest that a portion of particles that deposit on the conducting airways can be retained for long periods of time, or indefinitely.

Long-term retention and clearance patterns for radioactive particles that deposit in the head airways and TB region must be thoroughly evaluated because of the implications of this information for respiratory tract dosimetry and risk assessment (James et al., 1991; Johnson and Milencoff, 1989; Roy, 1989; ICRP, 1994). Similar concerns exist for non-radioactive particles that might be cytotoxic or elicit inflammatory, allergic, or immune responses at or near retention sites in conducting airways.

10.6.4.2 Alveolar Region

Model projections are possible for the A region using the cumulative information in the scientific literature relevant to deposition, retention, and clearance of inhaled particles. Table 10-16 summarizes reasonable approximations for physical alveolar clearance parameters for six laboratory animal species. Alveolar clearance curves produced using the parameters in Table 10-16 agree with curves produced using the parameters in Table 10-14. An advantage to using the parameters in Table 10-16 is that they separate physical clearance from the A region into its two components, physical clearance via the mucociliary clearance pathway to the GI tract and clearance to TLNs. To model the biokinetics of a specific type of particle in the A regions of these laboratory animal species, the physical clearance parameters in Table 10-16 were used in conjunction with a dissolution-absorption parameter to derive rates for effective clearance from the A region. As explained below, biokinetic modeling for particles deposited in the A region of humans was done using the new ICRP66 respiratory tract model (ICRP66, 1994). To model the alveolar biokinetics of a specific type of particle, the physical clearance parameters in Table 10-16 are used in conjunction with a dissolution-absorption parameter to derive rates for effective clearance from the A region.

TABLE 10-16. PHYSICAL CLEARANCE RATES[a] FOR MODELING ALVEOLAR CLEARANCE OF PARTICLES INHALED BY SELECTED MAMMALIAN SPECIES

Species	Clearance via Mucociliary Transport Pathway	Clearance to Thoracic Lymph Nodes
Mouse[b]	$0.023 \exp^{-0.008t} + 0.0013$	$0.0007 \exp^{-0.5t}$
Rat[b], Syrian hamster[c]	$0.028 \exp^{-0.01t} + 0.0018$	$0.0007 \exp^{-0.5t}$
Guinea pig[b]	$0.007 \exp^{-0.03t} + 0.0004$	0.00004
Monkey[d], dog[b]	$0.008 \exp^{-0.022t} + 0.0001$	0.0002

[a]Fraction of existing alveolar burden physically cleared per day.
[b]Adapted from Snipes (1989)
[c]Clearance rates assumed to be the same as for rats.
[d]Clearance rates assumed to be the same as for dogs.

10.7 APPLICATION OF DOSIMETRY MODELS TO DOSE-RESPONSE ASSESSMENT

For the purposes of this document an attempt was made to ascertain whether dosimetry modeling can provide insight into the apparent discrepancies between the epidemiologic and laboratory animal data, to identify plausible dose metrics of relevance to the available health endpoints, and to identify modifying factors that may enhance susceptibility to inhaled particles. In order to accomplish these objectives, this section presents an application of dosimetry modeling to data typically available from the epidemiologic and laboratory animal studies. Choice of a dosimetry model for humans and laboratory animals, respectively, is discussed and these models are used to simulate deposition and retained doses of various exposures. Different dose metrics and their relevance to observed health endpoints are also discussed.

Application of the chosen dosimetry models to calculate these estimates are intended to illustrate the potential influence dosimetry may have on estimation of dose to provide a linkage between the exposure and the available epidemiologic and toxicologic data. At present, respiratory tract dosimetry must rely on many simplifications and empiricisms, but even a somewhat rudimentary effort will assist in linking dose to effects and in species extrapolations. As more information on mechanistic determinants of dose, target tissues, and target dose and tissue interaction relationships become available, the more complex and

realistic the dosimetry construct will become. It is foreseen that choice of dose metrics will go beyond dependence on average mass or number concentration in the future as physiologically-based models become available. The human and laboratory animal models chosen for the simulations represent semi-empirical and empirical approaches to characterizing the available deposition and retention data. Default values for key parameters such as ventilation rate and body weight have been used in these simulation exercises. Disagreement with the limited published deposition and retention data is considered to be within the known variability among these parameters as well as biological detectability of the current state of measurement. As with any data-driven process, when additional data become available, the model structures can be reviewed and revised as appropriate. Additional experimental measurements would provide more information to strengthen the predictions and provide better description of intersubject and interspecies variability.

10.7.1 General Considerations for Extrapolation Modeling

Major factors that affect the disposition (deposition, uptake, distribution, metabolism, and elimination) of inhaled particles include the physicochemical properties of the particles (e.g., particle diameter, distribution, hygroscopicity) and anatomic (e.g., upper respiratory tract architecture, regional surface areas, airway diameters, airway lengths, branching patterns) and physiologic (e.g., ventilation rates, clearance mechanisms) parameters of individual mammalian species. The relative contribution of each of these factors is a dynamic relationship. Further, the relative contribution of these determinants is also influenced by exposure conditions such as concentration and duration. A comprehensive description of the exposure-dose-response continuum is desired for accurate extrapolation. Therefore, a dosimetry model should incorporate all of the various deterministic factors into a computational structure. Clearly, many advances in the understanding and quantification of the mechanistic determinants of particle disposition, toxicant-target interactions, and tissue responses (including species sensitivity) are required before an overall model of pathogenesis can be developed for a specific aerosol. Such data exist to varying degrees, however, and may be incorporated into less comprehensive models that nevertheless are useful in describing delivered doses or in some cases, target tissue interactions.

10.7.1.1 Model Structure and Parameterization

Data on the mechanistic determinants of particle disposition, toxicant-target interactions, and tissue responses to incorporate into a model vary in degree of availability for chemicals and animal species. An ideal theoretical mathematical model to describe particle deposition would require detailed information on all of the influential parameters (e.g., respiratory rates, exact airflow patterns, complete measurement of the branching structure of the respiratory tract, alveolar region mechanics) across different humans or across various laboratory species of interest. An empirical model (i.e., a system of equations fit to experimental data) is an alternative approach. A third approach, the hybrid approach adopted in ICRP66, is to fit a system of empirical equations to the results of theoretical modeling. Depending on the relative importance of these various mechanistic determinants, models with less detail may be used to adequately describe differences in respiratory dosimetry for the purposes of extrapolation.

An understanding of the bases for model structures also allows development of a framework for the evaluation of whether one available model structure may be considered optimal relative to another. A model structure might be considered more appropriate than another for extrapolation when default assumptions or parameters are replaced by more detailed, biologically-motivated descriptions or actual data, respectively. For example, a model could be preferred if it incorporates more chemical or species-specific information or if it accounts for more mechanistic determinants. Empirical models may differ in the quality or appropriateness of the data used to fit the descriptive equations. These considerations are summarized in Table 10-17.

The sensitivity of the model to differences in structure may be gauged by their relative importance in describing the response function for a given chemical. For example, a model that incorporates many parameters may not be any better at describing ("fitting") limited response data than a simpler model.

10.7.1.2 Intraspecies Variability

There are essentially three areas of concern in assessing the quality of epidemiologic or toxicity data. These involve the design and methodological approaches for (1) exposure

TABLE 10-17. HIERARCHY OF MODEL STRUCTURES FOR DOSIMETRY AND EXTRAPOLATION

Optimal model structure
Structure describes all significant mechanistic determinants of particle disposition, toxicant-target interaction, and tissue response
Uses chemical-specific and species-specific parameters
Dose metric described at level of detail commensurate with the epidemiologic or toxicity data
Default model structure
Limited or default description of mechanistic determinants of particle disposition, toxicant-target interaction, and tissue response
Uses categorical or default values for chemical and species parameters
Dose metric at generic level of detail

Source: Adapted from U.S. Environmental Protection Agency (1994); Jarabek (1995).

measures, (2) effect measures, and (3) the control of covariables and confounding variables. Although these topics are discussed in detail in other chapters, it is also important to consider these concerns when evaluating potential dosimetry models for extrapolation of epidemiologic or toxicity data. For example, although the epidemiologic investigations attempt to relate an exposure to a given health effect, the way the exposure is characterized may influence the choice of an appropriate dosimetry model. Characterization of a particular health effect in a human population may include pre-existing pathologic conditions (e.g., lung disease) that may alter inhalation dosimetry and have implications for model choice. The broad genetic variation of the human population in processes related to chemical disposition and tissue response (e.g., age, gender, disease status) may cause individual differences in sensitivity to inhaled aerosols. Sensitivity analyses could be used to determine ranges of dosimetry model outputs for specific ranges of input for various parameters (e.g., range in ventilation rate due to gender).

10.7.1.3 Extrapolation of Laboratory Animal Data to Humans

Toxicological data in laboratory animals typically can aid the interpretation of human clinical and epidemiological data because they provide concentration- and duration-response information on a fuller array of effects and exposures than can be evaluated in humans.

However, historically, use of laboratory animal toxicological data has been limited because of difficulties in quantitative extrapolation to humans. The various species used in inhalation toxicology studies do not receive identical doses in comparable respiratory tract regions (ET, TB, A) when exposed to the same aerosol (same composition, $\mu g/m^3$, MMAD, σ_g). Such interspecies differences are important because the adverse toxic effect is likely more related to the quantitative pattern of deposition within the respiratory tract than to the exposure; this pattern determines not only the initial respiratory tract tissue dose but also the specific pathways by which the inhaled particles are cleared and redistributed.

Both qualitative and quantitative extrapolation of laboratory animal data to humans are of interest. Qualitative extrapolation refers to the "class" of the effects. For example, if the function of rabbit alveolar macrophages is depressed by sulfuric acid, will it also be depressed in humans, albeit at an unknown exposure? This type of extrapolation is limited to known homologous effects. For example, given the similarities in human and laboratory animal alveolar macrophages, and likely toxicity mechanisms, the qualitative extrapolation is reasonable. However, in some cases, the homology is not understood adequately. For example, what is the laboratory animal model homology to the mortality effects observed in the epidemiological studies? Would PM exposures of aged animals or animal models of respiratory or cardiac disease states more closely mimic the mortality observed among the elderly or those with pre-existing cardiopulmonary disease? Several hypotheses exist, but at present there is inadequate evidence for concensus.

Once a qualitative extrapolation has been justified, a quantitative extrapolation can be initiated. In order for the laboratory animal data to be useful to the risk assessment of PM, interspecies extrapolation should account for differences in particle dosimetry and species sensitivity. Dosimetry, here, is used broadly to represent the effective dose to target site which may be some complex combination of regional delivered or retained particle burdens. Given the identical exposure, these particle burdens may be different in different species. Even if there is a comprehensive understanding of dose, there still needs to be an understanding of species differences in sensitivity to that dose. For example, perhaps one species has more efficient repair or chemical defense mechanisms than another, making that one species less sensitive to a given dose.

10.7.2 Dosimetry Model Selection

Available deposition models for humans and laboratory animals were presented in Section 10.5.1 and 10.5.2, respectively. Clearance models, required to calculate retained doses, were discussed in Section 10.6. This section focuses on modeling efforts intended to present informative and comparative data relevant to lung burdens that result in humans and laboratory animals as a consequence of acute and chronic inhalation exposures. The information and predictions are intended to illustrate examples of approaches to lung dosimetry, metrics of deposited and retained particle burdens, and species similarities and differences that influence exposure and dose metrics.

10.7.2.1 Human Model

The theoretically-based, semi-empirical lung deposition model of the International Commission on Radiological Protection (ICRP66, 1994) was chosen and used to model the dosimetry of inhaled particles in humans (Sections 10.7.4 and 10.7.5 below). A distinct advantage of this model is that it incorporates both deposition and clearance mechansisms so that both deposited and retained particles burdens can be calculated. LUDEP® software version 1.1 was used to run the ICRP66 1994 model simulations (National Radiological Protection Board, 1994).

Although the highly-detailed theoretical models described in Section 10.5 might allow prediction to more localized regions of the respiratory tract, information about the dimensions of the numerous gross and microscopic structures of the respiratory tract are extremely limited. Human experimental data are still available only for gross regional deposition, for the adult Caucasian male, and for a limited range of particle size (d_{ae} from about 1 μm to 10 μm), making validation of the most detailed theoretical models impossible at the present time. For these reasons, the analysis of respiratory tract deposition by gross anatomical region adopted by the ICRP was viewed as advantageous. The parametric analysis of regional lung desposition, developed by Rudolf et al. (1986, 1990) and described in Section 10.5, was used to represent the results of complex theoretical modeling by relatively simple algebraic approximations. A theoretical model of gas transport and particle deposition (Egan et al., 1989) was applied to apportion particle deposition among the lower respiratory tract regions (BB, bb, AI — see Section 10.6), and to quantify the effects of lung

size and breathing rate. The structure of the respiratory tract is represented explicitly by a morphometric anatomical model as described in Table 10-3 and Figure 10-4. The 1994 ICRP model reasonably describes the experimental data relating total thoracic deposition to particle size and breathing behavior. The model also succeeds in simulating the variation of regional deposition with particle size and breathing pattern that was inferred by Stahlhofen et al. (1980,1983) from their measurements of thoracic depostion and retention. In common with earlier theoretical models of Yeh and Schum (1980) and Yu and Diu (1982b), the 1994 ICRP model predicts less thoracic deposition for particles in the range of d_{ae} from 1 μm to 5 μm than the median values reported by Lippmann (1977) and Chan and Lippmann (1980). These data are crucial since they represent the largest group of experimental subjects studied to date. However, as described in Appendix 10A, according to the analysis in ICRP66 (1994), there is direct experimental evidence (Gebhart et al., 1988) that particulate material used in the New York University (NYU) studies exhibits a degree of hygroscopic growth in the respiratory tract. When allowance is made in the deposition calculation for these supplementary data, the key set of experimental measurements from NYU is also found to support the 1994 ICRP66 deposition model. The problem of time-dependent functions to describe clearance from the various regions in the respiratory tract was overcome by using a combination of compartments with constant rates of clearance. Clearance from each region by three routes (absorption into blood, transport to GI tract, and transport to lymphatics) is accomplished by pathways with assigned rate constants.

Mathematical models such as the ICRP66 model do not provide site-specific dosimetry at the level of individual lung lobes, but the objective of this exercise is to provide useful insights about dose metrics such as average concentrations and average numbers of particles per unit area of respiratory regions. The ICRP model provides average concentration or average number values on a regional basis, i.e., mass or number deposited or retained in the ET, TB, or A regions. An important aspect of modeling and dosimetry is to relate the modeling effort to the level or accuracy of measurements. Neither the available deposition and clearance data nor the response data such as the mortality effects provide a level of detail that support more physiologically-based parameters and compartments.

The available deposition data were from radioactive tracer studies, in which accurate measurements were obtained at very low particulate mass burdens. As such, the particle

mass deposited in the respiratory tract was negligible, and did not introduce the possibility of experimental artifact due to particle overload phenomena. Biphasic or multiphasic clearance processes do not necessarily imply specific physiologic associations. The ICRP model makes use of convenient mathematical approaches to vary the rates of specific processes involved in clearance. The time dependence of clearance processes (both physical and dissolution-absorption) may well be determined by a decrease in the availability of the particles, e.g., because of (1) burial of the particles in the interstitial tissue, (2) sequestering in macrophages in areas that have low probability of physical clearance, or (3) altered dissolution-absorption rates related to physical or chemical changes in the particle with time.

Both the NCRP and ICRP had the benefit of contributions from respected investigators in respiratory tract toxicology and biomedical aerosol research. Similar mathematical assessments were arrived at by both commissions, although detailed calculations for specific radionuclides can be different. Comparisons between the models presented earlier and in Appendix 10A show that the behavior of the models are quite comparable, that is, the predicted deposition fraction for a given particle size is similar if the models use the same ventilation parameters as input. In fact, in order to ensure a uniform course of action that provides a coherent and consistent international approach, the NCRP recommends adoption of the ICRP 1994 model for modeling the effects of exposure for radiation workers and the public (e.g., for computing reference levels of annual intake and derived reference air concentrations corresponding to recommended dose limits).

Some of the human parameter values used in the ICRP66 model (ICRP66, 1994) and the LUDEP® software are provided in Appendix 10B. Surface area values were derived by the ICRP based on the morphometry provided previously in Table 10-3. LUDEP® allows simulations of either normal augmenter or mouth breather adult male humans. The proportion of nasal airflow for these two types of breathing at different levels of activity previously provided in Figure 10-27 and Table 10-11 in Section 10.5. The levels of activity to apportion nasal airflow are the same as those used to construct the three different activity patterns (general population; worker, light work; and worker, heavy work) shown in Table 10B-1.

10.7.2.2 Laboratory Animal Model

The particle dosimetry model of Ménache et al. (1996) descirbed in Section 10.5.2 was chosen to calculate deposited dose estimates for rats as an illustration of dosimetric adjustment for laboratory animal species. Attributes of the model that were viewed as especially advantageous for this exercise included the detailed measurements made in all tissues that served as the source of deposition data (Raabe et al., 1988); that the deposition data were available for unanesthetized, freely breathing animals; and that inhalability was accounted for and used to adjust the logistic function to describe deposition efficiency. This model represents a revised version of previous models (Miller et al., 1988; Jarabek et al., 1989, 1990) that have been useful to develop inhalation reference concentration (RfC) estimates for dose-response assessment of air toxics (U.S. EPA, 1994). The same approach will be used to calculate deposited doses as discussed below in greater detail (Section 10.7.4). The range for application of the Ménache et al. (1996) model to interspecies extrapolation was restricted to 1 to 4 μm MMAD because this is the range that had the most deposition data for model development and it is also the range most likely of use for evaluating the available inhalation toxicology investigations.

For calculation of retained doses, the simulation model based on Pritsker (1974) and described in Section 10.6 was used. This clearance model was applied to output of the Ménache et al. (1996) deposition model in order to calculate retained dose as discussed below in Section 10.7.5.

The broad spectrum of mammals used in inhalation toxicology research have body weights ranging upwards from a few grams to tens of kg; these mammals also exhibit a broad range of respiratory parameters. Table 10B-2 in Appendix 10B lists body weights, lung weights, respiratory minute ventilation and respiratory tract region surface areas for six laboratory animal species. Lung weights and ventilation parameters are important variables for inhalation toxicology because these parameters dictate the amounts of inhaled materials potentially deposited in the lung, as well as the specific alveolar burdens (mass of particles/g lung) that will result from inhalation exposures. The inverse relationship between body size and metabolic rate is demonstrated by the values for respiratory minute ventilation and body weight or lung tissue volume. For example, liters of air inhaled per minute per gram of lung is about 20 times higher for resting mice than for resting humans, which is an important

factor to consider relative to potential amounts of aerosol deposited in the respiratory tract per unit time during inhalation exposures.

10.7.3 Choice of Dose Metrics

As discussed in the preceding sections, inhaled dose, especially to different regions or locations within the respiratory tract, is not necessarily related linearly to the exposure concentration. For this reason, an internal dose to characterize the dose-response relationship of PM is desired. In general, the objective is to provide a metric that is mechanistically-motivated by the observed response. Unfortunately, at this point in time, the crucial definition and determination of the relevant dose has not been accomplished for PM. Mechanistic determinants of the observed health effects have not been adequately elucidated. The health effects data discussed later (Chapter 11, 12, and 13) include effects that could be characterized as either "acute" (e.g., effects associated with mortality) or "chronic" (e.g., morbidity or laboratory animal pathology after two-year bioassays). Dose may be accurately described by particle deposition alone if the particles exert their primary action on the surface contacted (Dahl et al., 1991), i.e., deposited dose may be an appropriate metric for acute effects. For longer-term effects, the initially deposited dose may not be as decisive a metric since particles clear at varying rates from different lung compartments. To characterize these effects, a retained dose that accounts for differences between deposition and clearance is more appropriate.

Conventionally and conveniently, doses usually are expressed in terms of particle mass (gravimetric dose). However, when different types of particles are compared, doses may be more appropriately expressed as particle volume, particle surface area, or numbers of particles, depending on the effect in question (Oberdörster et al., 1994). For example, the retardation of alveolar macrophage-mediated clearance due to particle overload appears to be better correlated with phagocytized particle volume rather than mass (Morrow, 1988). As shown in Figures 10-2 and 10-3, the smaller size fractions of aerosols are associated with greater amounts of particles when characterized by surface area or by number rather than by mass. That is, concentrations in this size fraction are very small by mass but extremely high by number. The need to consider this is accentuated when the high rate of deposition of small particles in the lower respiratory tract (TB and A regions), the putative target for the

mortality and morbidity effects of PM exposures, is also taken into account. Anderson et al. (1990) have shown that the deposition of ultrafine particles in patients with COPD is greater than in healthy subjects.

Miller et al. (1995) recently investigated considerations for both intraspecies and interspecies dosimetry. Using a multipath dosimetric model, simulations for different particle sizes (0.1, 1, and 5 μm) were performed and different dose metrics calculated for the rat and both normal and compromised human lung status. A summary table of this exercise is provided as Table 10-18. These simulations support the conclusion that particle number per various anatomical normalizing factors indicate a need to examine the role of fine particles in eliciting acute morbidity and mortality, particularly in patients with compromised lung status (Miller et al., 1995).

For the present document, average deposited particle mass burden in each region of the respiratory tract has been selected as the dose metric for "acute" effects in both humans and laboratory animals. Average retained particle mass burden in each region for humans and in the lower respiratory tract for laboratory animals has been selected as the dose metric for "chronic" effects. These choices were dictated by the selection of the dosimetry models and the availability of anatomical and morphometric information.

Because mass may not be the appropriate metric, especially to characterize effects of the fine fraction, average particle number burdens and the number of particles deposited per day were calculated in addition for humans. An attempt to address the variability due to differences in the population was made by calculating deposited particle mass burdens in each region for eight different demographic groups that included a range of ages and one selected for cardiopulmonary symptoms.

10.7.3.1 Interspecies Extrapolation

In order to gain insight on species similarities and differences that may account for the apparent discrepancies between epidemiologic and laboratory animal data, interspecies adjustments to the observed exposure levels must be made for the dose metrics selected for "acute" and "chronic" effects. This section discusses an approach to calculate human equivalent concentration (HEC) estimates based on the observed laboratory animal toxicological data.

TABLE 10-18. SPECIES COMPARISONS BY MILLER ET AL. (1995) OF VARIOUS DOSE METRICS AS A FUNCTION OF PARTICLE SIZE FOR 24-HOUR EXPOSURES TO 150 $\mu g/m^3$

Particle Size	Dose Metric	Rat	Human Lung Status[a] Normal	Human Lung Status[a] Compromised	Ratio: Human/Rat Normal	Ratio: Human/Rat Compromised
	Mass/unit area	$3.74\text{-}3.76 \times 10^{-3}$	5.0×10^{-4}	NC[d]	0.13	NC[d]
0.1 μm	No. deposited[b]	1.2×10^{10}	5.9×10^{11}	4.3×10^{11}	49	37
	No./unit surface area	7.1×10^{6}	9.5×10^{5}	2.8×10^{6}	0.1	0.4
	No./ventilatory unit	4.9×10^{6}	1.8×10^{7}	5.3×10^{7}	4	11
	No./alveolus[c]	303-598	1,190-1,930	3,570-5,790	2-5	6-15
	No./macrophage[c]	262-399	100-61	298-482	0.3-0.6	0.8-1.8
1 μm	Mass/unit area	$1.1\text{-}1.2 \times 10^{-3}$	2.8×10^{-4}	NC[d]	0.23-0.25	NC[d]
	No. deposited	3.5×10^{6}	3.3×10^{6}	2.4×10^{8}	92	69
	No./unit surface area	2,130	532	1,590	0.3	0.8
	No./ventilatory unit	1,470	9,910	29,700	7	20
	No./alveolus[c]	0.12-0.18	0.7-1.1	2.0-3.3	4-9	11-28
	No./macrophage[c]	0.08-0.12	0.06-0.09	0.2-0.3	0.5-1.2	1.4 -3.5
5 μm	Mass/unit area	$2.8\text{-}4.4 \times 10^{-4}$	9.1×10^{4}	NC[d]	2.09-3.23	NC[d]
	No. deposited	7.1×10^{3}	8.5×10^{6}	6.4×10^{6}	1,195	897
	No./unit surface area	4	14	42	3.2	9.7
	No./ventilatory unit	3	260	780	88	263
	No./alveolus[c]	0.0002	0.02-0.03	0.05-0.09	49-120	145-359

A HEC would be calculated by

$$\text{HEC } (\mu g/m^3) = \text{NOAEL}_{[ADJ]} \ (\mu g/m^3) \times DAF_r, \qquad (10\text{-}48)$$

where the $NOAEL_{[ADJ]}$ is the no-observed-adverse-effect level (or other effect level) of the laboratory animal study (this level, if from an intermittent exposure regimen, is often adjusted for the number of hours per day and days per week (#/24 x #/7) in order to model a continuous exposure) and DAF_r is a dosimetric adjustment factor for a specific respiratory tract region, r (ET, TB, A). The DAF_r is either the regional deposited dose ratio ($RDDR_r$) for "acute" effects of deposited particles or the regional gas dose ratio ($RGDR_r$) for "chronic" effects of retained particles. The DAF_r is a multiplicative factor that represents the laboratory animal to human ratio of a specific inhaled particle burden. The HEC is expected to be associated with the same delivered particle burden to the observed target tissue as in the laboratory animal species. A DAF_r above the value of 1.0 indicates that the human receives a relatively smaller deposited or retained particle burden than the particular laboratory animal species. Values of the DAF_r below 1.0 indicate that the human receives a relatively larger deposited or retained particle burden than the laboratory animal species, and application of the DAF_r would adjust the resultant HEC lower than the laboratory animal exposure level.

For deposited particle burdens, regional deposited dose (RDD_r) can be calculated as

$$\mathbf{RDD_r = 10^{-3} \times C_i \times \dot{V}_E \times F_r}, \qquad (10\text{-}49)$$

where:

RDD_r = dose deposited in region r (μg/min),
C_i = concentration ($\mu g/m^3$),
$\dot{V}_E$ = minute ventilation (L/min), and
F_r = fractional deposition in region r.

If the RDD in laboratory animals is expressed relative to humans, the resultant regional deposited dose ratio ($RDDR_r$) can be used as the DAF_r in Equation 10-48 to adjust an inhalation particulate exposure in a laboratory species to a predicted HEC that would be

expected to be associated with the same particle burden delivered to the r^{th} region of the respiratory tract. The $RDDR_r$ can be calculated as a series of ratios

$$DDR_r = \frac{(10^{-3} \times C_i)_A}{(10^{-3} \times C_i)_H} \times \frac{(\text{Normalizing Factor})_H}{(\text{Normalizing Factor})_A} \times \frac{(\dot{V}_E)_A}{(\dot{V}_E)_H} \times \frac{(F_r)_A}{(F_r)_H} \quad (10\text{-}50)$$

where the normalizing factor can be selected based on consideration of the mechanism of action. Because poorly soluble particles deposit along the surface of the respiratory tract, the surface area of an affected respiratory tract region (e.g., TB or A region) could be used as the normalizing factor. For the purposes of calculating the $RDDR_r$, the exposure concentration for the laboratory animal (A) and human (H) are assumed to be the same because it is assumed that the observed effect in the laboratory animal is relevant to human health risk. The $RDDR_r$ is used as a factor to adjust for interspecies differences in delivered dose under the same exposure scenario. The first term in Equation 10-50, therefore, equals one and will not be discussed further. The last term, the ratio of deposition fractions in a given respiratory region, (F_r), is calculated using the respective human and laboratory animal dosimetry models.

Because the ICRP66 model utilizes an activity pattern, Equation 10-50 must be modified to account for the fraction of time spent at each different ventilation rate, corresponding to each different activity levels, as

$$RDDR_{r_{[ACT]}} = \frac{a}{t_{[1]} \times \dot{V}_{E_{H[1]}} \times F_{r_{H[1]}} + t_{[2]} \times \dot{V}_{E_{H[2]}} \times F_{r_{H[2]}} + \ldots + t_{[n]} \times \dot{V}_{E_{H[n]}}} \quad (10\text{-}51)$$

where $t_{[i]}$ is the fractional time spent breathing minute volume [i],

$$t_{[1]} + t_{[2]} + \ldots + t_{[n]} = 1, \quad \text{and} \quad (10\text{-}52)$$

$$a = \frac{(\text{Normalizing Factor})_H}{(\text{Normalizing Factor})_A} \times \dot{V}D_{E_A} \times F_{r_A}, \quad (10\text{-}53)$$

where $\dot{V}D_{E_A}$ is a daily average ventilation rate (L/min × 1440 min/day). It should be noted that the human denominator is the fractional deposition value output from the ICRP model simulations using the LUDEP® software using an activity pattern.

Although clearance is dependent on the site of initial deposition, calculation of retained dose is probably more appropriate for assessing chronic heatlh effects. Different normalizing factors such as retained mass per region, retained mass per surface area, or retained mass per other available morphometric information may be worthwhile to explore. The regional retained dose ratio ($RRDR_r$) for interspecies dosimetric adjustment is calculated as a series of five ratios

$$RRDR_r = \frac{(10^{-3}\times Ci)_A}{(10^{-3}\times Ci)_H} \times \frac{(\text{Normalizing Factor})_H}{(\text{Normalizing Factor})_A} \times \frac{(\dot{V}_E)_A}{(\dot{V}_E)_H} \times \frac{(F_r)_A}{(F_r)_H} \times \frac{(AI_t)_A}{(AI_t)_H} \quad (10\text{-}54)$$

where:

$RRDR_r$ = relative μg of particles retained in region (r),
Ci = exposure atmosphere concentration ($\mu g/m^3$),
Normalizing Factor = lung weight (g),
$\dot{V}_E$ = minute ventilation (L/min),
F_r = fractional aerosol deposition in region r, and
(AI_t) = relative accumulated alveolar interstitial burden of particles as a function of time from the start of a chronic exposure.

Again, since the ICRP66 model allows simulation of an activity pattern, Equation 10-54 must be adjusted to account for the fraction of time spent at each different ventilation rate corresponding to different activity levels so that

$$RRDR_{r_{[ACT]}} = \frac{a}{t_{[1]} \times \dot{V}_{E_{H[1]}} \times F_{r_{H[1]}} \times (AI_t)_{H[1]} \times t_{[2]} \times \dot{V}_{E_{H[2]}} \times F_{r_{H[2]}} \times (AI_t)_{H[2]} + \ldots + t_{[n]} \times \dot{V}_{E_{H[n]}} \times (AI_t)_{H[n]}} \quad (10\text{-}55)$$

where $t_{[i]}$ is the fractional time spent breathing at minute ventilation [i],

$$t_{[1]} + t_{[2]} + \ldots + t_{[n]} = 1, \text{ and} \tag{10-56}$$

$$a = \frac{(\text{NormalizingFactor}_r)_H}{(\text{NormalizingFactor}_r)_A} \times (\dot{V}D_E)_A \times (Fr)_A \times (AI_t)_A \ , \tag{10-57}$$

and $(\dot{V}D_{E_A})$ is a daily average ventilation rate (L/min × 1440 min/day).

The relative accumulated alveolar interstitial burden of particles as a function of time from the start of a chronic exposure must be calculated for specific exposure scenarios to account for species differences in clearance, as well as the dissolution-absorption characteristics of the inhaled particles. This ratio is not a constant and must be calculated for the chronic exposure time of interest. Physical clearance functions and dissolution-absorption rates for particles deposited in the A region are used to integrate daily deposition and clearance over the chronic exposure time period of interest. The equations for laboratory animals are derived using the information in Table 10-16. Physical clearance parameters for humans are in the ICRP model (ICRP66, 1994) and the calculation of A burden for humans can be made using LUDEP®.

Calculating these ratios (either deposited or retained) depends on particle diameter (MMAD) and distribution (σ_g) but not on aerosol concentration, i.e., it assumes no altered deposition or clearance due to exposure concentration or chemical-specific toxicity.

The calculation of the DAF_r currently uses point estimates for all the terms used to construct the ratios, that is, a default $\dot{V}_E$ for each species, a default regional surface area or lung weight for the normalizing factor, and an estimate of fractional deposition or retained particle burden. These single values are assumed to be representative of the average value of that term for a member of the laboratory animal species or human population. As discussed in the previous sections of this chapter, there are many sources of intraspecies variability that contribute to the range of responses observed to a given external exposure to an inhaled toxicant. Host factors may affect both the delivered dose of the toxicant to the target tissue as well as the sensitivity of that tissue to interaction with the toxicant. The procedures described in this interspecies extrapolation section could provide some limited capability to

examine the effects of population variability on the DAF_r by changing the default $\dot{V}_E$ and surface areas or lung weights in an iterative fashion. However, because of correlations between $\dot{V}_E$, surface area, and lung weight, such changes should be made with caution. Confidence intervals were provided on the parameters for the deposition efficiency equations. Iterative computational procedures could be used to generate evelopes of regional fractional deposition that could be used with distributions of $\dot{V}_E$, surface areas, and lung weights to provide ranges of DAF_r estimates. Actual implementation of this procedure is not straightforward due to the complex nature of the correlation structures. Future versions of the deposition and clearance models used to calculate the laboratory animal species values could estimate distributions that reflect the range of available data for key parameters.

10.7.4 Choice of Exposure Metrics

10.7.4.1 Human Exposure Data

Ambient exposure data provided elsewhere in Chapter 3 of this document were selected to represent typical human exposures. Three different aerosols were selected as presented in Appendix 10C. As discussed in Chapter 3, it is not known at this time whether the intermodal mode for the trimodal aerosols is real or whether it is an artifact of sampling procedures.

The first is the trimodal aerosol shown in Figure 10C-1. Table 10C-1 shows the upper size cut (in μm) for various particle size intervals based on the distribution of particle count, surface area, mass, or aerodynamic diameter (d_{ae}). Recall from Section 10.2 that the 50% size cut for each of these diameters would be the respective median diameter of the distribution, i.e., the 50% size-cut diameter of the d_{ae} is the MMAD. Table 10C-2a,b,c shows the particle number, surface, area, and mass distribution, respectively, for the aerosol from Figure 10C-1. The distribution of particle mass in Table 10C-2c was used as input to the human dosimetry (ICRP66, 1994) model to estimate total particle mass deposition.

The two trimodal aerosols depicted in Figure 10C-2, panel (a) and (b) for Philadelphia and Phoenix respectively, were also chosen and treated similarly. Table 10C-3 shows the upper size cut (in μm) for various particle size intervals from the Philadelphia aerosol (Panel a), based on the distribution of particle count, surface area, mass, or aerodynamic diameter (d_{ae}). Table 10C-4a,b,c shows the particle number, surface area, and mass

distribution, respectively, from Figure 10C-2(a). The distribution of particle mass in Table 10C-4c was used as input to the human dosimetry model (ICRP, 1994) to estimate total particle mass deposition. Tables 10C-5 and 10-C6a,b,c are analogous to Tables 10-C3 and 10C-4a,b,c but show the data for Phoenix (Figure 10C-2b).

10.7.4.2 Laboratory Animal Data

As noted previously, the range of application for the Ménache et al. (1996) model was limited to that typically used in laboratory animal studies that are the basis of the toxicity data in Chapter 11. For calculation of deposited doses, fractional deposition was estimated for a range of particle diameters (d_{ae}) and two distributions (σ_g), one representing a relatively monodisperse ($\sigma_g = 1.3$) and the other a polydisperse ($\sigma_g = 2.4$) aerosol. Deposited doses for two different particle diameters and distributions were then used in clearance models to calculate retained doses (see Section 10.7.5).

10.7.5 Deposited Dose Estimations

The respective models discussed in Section 10.7.1 were used to estimate deposition in each of the respiratory tract regions. Note that the ICRP66 human model divides the ET region into compartments, ET_1 and ET_2. The ICRP66 model also divides the TB region into two compartments, the bronchi (BB) and bronchiole (bb). The alveolar interstitial (AI) compartment is equivalent to the A region. When compared to the laboratory animal data, deposition fractions for ET_1 and ET_2 were summed to calculate ET deposition. Likewise, the BB and bb deposition fractions were summed to calculate the TB fraction.